Optical characterization of semiconductors using photo reflection spectroscopy

by

Rheinhardt Hendrik Sieberhagen

submitted in partial fulfilment of the requirements for the degree

Magister Scientiae

in the Faculty of Natural and Agricultural Sciences
University of Pretoria
Pretoria
February 2002

Optical characterization of semiconductors using photo reflection spectroscopy

by

Rheinhardt Hendrik Sieberhagen

Supervisor: Professor D.J. Brink
Faculty: Natural and Agricultural Sciences
Department: Physics
Degree: Magister Scientiae

Abstract

The study of semiconductor materials and more recently, artificially structured materials, is important for both scientific and industrial purposes. Many techniques have been developed to characterize the electronic properties of these materials. Optical characterization is a popular approach to this field of study, as the absorption or reflection of incident photons is directly related to the band structure of a semiconductor material.

When measuring the absolute reflectivity or absorptivity, the resulting spectrum is often rather featureless, making it difficult to observe band structure features. This led to the invention of modulation spectroscopy techniques where the derivative of the absorptivity or reflectiviy of a semiconductor material with respect to some experimental parameter, is evaluated. Weak features in the absolute spectrum are thus enhanced, making the identification of band structure features easier.

This study describes the technique of photo reflection spectroscopy (commonly known as photoreflectance spectroscopy) where modulation is achieved optically. The theory behind photoreflectance spectroscopy is discussed in detail, whereafter the practical implementation is described. This is followed by measurements done on GaAs to do a basic comparison with published results. Finally, three different doping superlattices were investigated with this technique; including the influence that α-particle irradiation and consequent annealing have on the measured photoreflectance spectra.

Acknowledgements

I would like to thank my supervisor for his guidance during this study, and my family for their encouragement and support.

Contents

List of Tables

List of Figures

Chapter 1

Introduction

Artificially structured materials (ASM), such as quantum wells and superlattices, have been the subject of considerable theoretical and experimental studies for quite some time [1]. These microstructures are of technological and scientific interest because they exhibit properties that are significantly different from bulk materials. Furthermore, because of the flexibility offered by high-technology growth techniques, the chemical compositions, thicknesses and doping concentrations of the layers are design parameters. This allows the properties of ASM to be tuned for particular technological or basic science needs.

Many experimental techniques have been applied to the study of microstructures. One such technique is modulation spectroscopy. Modulation spectroscopy is a valuable experimental tool in the study of materials such as bulk semiconductors, quantum wells and superlattices. In general, one could measure the absorptivity or reflectivity with respect to some parameter, but in the case of modulation spectroscopy, the quantity of interest is $\Delta R(\lambda)/R(\lambda)$, where $\Delta R(\lambda)$ is the modulated reflectivity and $R(\lambda)$ is the unmodulated or *dc* reflectivity [2]. Modulation is achieved by applying a repetitive perturbation to the material being studied and because the optical properties of a material are fully described by the dielectric function, $\epsilon = \epsilon_1 + i\epsilon_2$, the effect of the modulation parameter on these properties must appear as a change in the real and the imaginary parts of the dielectric function.

Photoreflectance (PR) is an example of modulation spectroscopy. It is a contactless form of electromodulation in which the internal electric field of the sample is modulated by electron-hole pairs created by a modulated pump-beam (typically light from a small visible laser at a level of a few milliwatt).

The aim of this study was to construct a PR experimental arrangement and to use this to study bulk GaAs samples as well as three different doping superlattice samples. In addition to this, the three superlattice samples were particle-irradiated and afterwards annealed, to investigate the effect of radiation damage on the PR-spectra.

The basic outline of this dissertation is as follows: In chapter 2 the technique and theory of photoreflectance will be described. Following that, in chapter 3, the electronic structure and properties of doping superlattices will be explained. Chapter 4 is then devoted to describing the experimental technique of photoreflectance, followed by a description of the measurements that were carried out and a discussion thereof in chapter 5. Finally, some concluding remarks and suggestions for future research are provided in chapter 6.

References

[1] Glembocki O.J., Shanabrook B.V. in *The Spectroscopy of Semiconductors : SEMICONDUCTORS AND SEMIMETALS* Vol. 36 Chapter 4

[2] Shen H.,Parayanthal P., Liu Y.F., Pollak F.H, Rev. Sci. Instrum. **58**(8), (1987), p.1429

Chapter 2

The Technique of Photoreflectance

2.1 General Theory

2.1.1 Introduction

With modulation spectroscopy, the derivative of the absorptivity or reflectivity of a semiconductor material with respect to some parameter, is evaluated. Weak features that may have been difficult to observe in the absolute absorption or reflection spectrum are enhanced, as can be seen from the sharp derivative-like features of a resulting spectrum, as shown in figure 2.1 [1]. The modulation can be accomplished by varying some parameter of the sample or experimental system in a periodic fashion and measuring the corresponding normalized change in the optical properties.

In this study, the interest lies in a photoinduced variation in the built-in electric field in a sample. This is achieved by the technique of photoreflectance. This is a contactless technique in which a so-called pump-beam (usually a small laser operating in the visible spectrum) is used to photoinject electron-hole pairs, which modulate the built-in electric field of the microstructure under investigation. The pump-beam should therefore have a photon energy greater than the bandgap of the semiconductor.

Differential changes in the reflectivity can be related to a perturbation of

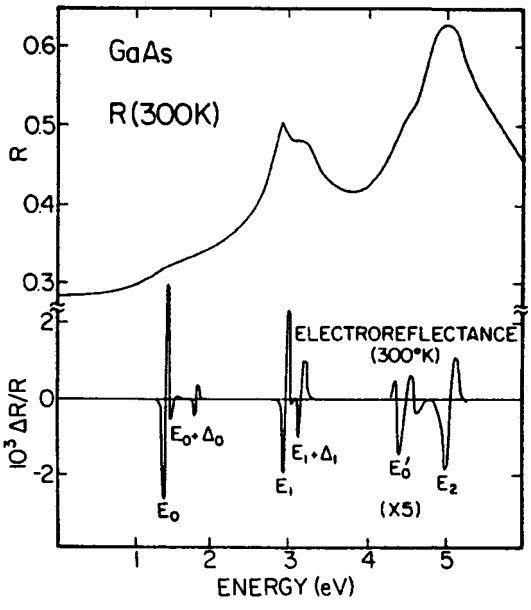

Figure 2.1: Typical reflectivity and electroreflectance spectra of GaAs.

the complex dielectric function in the following way

$$\frac{\Delta R}{R} = \alpha \Delta \epsilon_1 + \beta \Delta \epsilon_2 \tag{2.1}$$

where R is the reflectivity, $\Delta\epsilon_1$ and $\Delta\epsilon_2$ are the changes in the complex dielectric function, $\epsilon = \epsilon_1 + i\epsilon_2$, and α, β are the *Seraphin* coefficients, which are related to the unperturbed dielectric function [1][2]. In bulk materials, near the fundamental gap, $\beta \approx 0$ so that $\Delta R/R \approx \alpha \Delta \epsilon_1$. In multilayer structures, both $\alpha\Delta\epsilon_1$ and $\beta\Delta\epsilon_2$ have to be considered because of interference effects [1] [3].

2.1.2 Modulated Dielectric Function

The absorption of an incident photon due to the creation of an electron-hole pair is the fundamental process linking the band structure of a semiconductor to its optical properties. This link is defined by the probability of individual

absorption processes, the contribution of all such absorption processes possible at a given photon energy and the relationship of this sum to the macroscopic optical quantities [4].

A monochromatic flux of photons entering an absorbing medium in the plane $x = 0$, with an energy density $I(0)$, is reduced to $I(d)$ after reaching the plane $x = d$ according to

$$I(d) = I(0)e^{-K \cdot d} \tag{2.2}$$

where $K = (\omega/nc)\epsilon_2(\omega)$, is the absorption coefficient of the medium at angular frequency ω of the optical field, and ϵ_2 is the imaginary part of the dielectric function

$$\epsilon(\omega) = \epsilon_1(\omega) + i\epsilon_2(\omega). \tag{2.3}$$

The real and imaginary parts of this dielectric function are related to the optical constants n and k by

$$\epsilon = N^2 \tag{2.4}$$

or

$$\epsilon_1 = n^2 - k^2; \;\; \epsilon_2 = 2nk \tag{2.5}$$

where

$$N = n - ik. \tag{2.6}$$

The macroscopic quantity related to electronic transitions is the imaginary part, ϵ_2 of the dielectric function. The most direct way to determine ϵ_2, is by absorption measurements. In contrast to this, reflectance (at normal incidence) depends on both parts of the dielectric function

$$R = \left(\frac{N-1}{N+1}\right)^2 = \frac{(\epsilon_1^2 + \epsilon_2^2)^{\frac{1}{2}} - [2\epsilon_1 + 2(\epsilon_1^2 + \epsilon_2^2)^{\frac{1}{2}}]^{\frac{1}{2}} + 1}{(\epsilon_1^2 + \epsilon_2^2)^{\frac{1}{2}} + [2\epsilon_1 + 2(\epsilon_1^2 + \epsilon_2^2)^{\frac{1}{2}}]^{\frac{1}{2}} + 1} \tag{2.7}$$

The real and imaginary parts of the dielectric function are related by the *Kramers-Kronig* relations [4]

$$\epsilon_1(\omega_0) = 1 + \frac{2}{\pi}\int_0^\infty \frac{\omega \cdot \epsilon_2(\omega)}{\omega^2 - \omega_0^2}\, d\omega \tag{2.8}$$

and

$$\epsilon_2(\omega_0) = -\frac{2}{\pi}\int_0^\infty \frac{\epsilon_1(\omega)-1}{\omega^2-\omega_0^2}\,d\omega \tag{2.9}$$

A similar dispersion relation holds between real and imaginary parts of the reflection amplitude

$$r = |r|e^{i\phi}; R = |r^2| \tag{2.10}$$

$$\phi(\omega_0) = \frac{1}{2\pi}\int_0^\infty \ln\left|\frac{\omega-\omega_0}{\omega+\omega_0}\right| \frac{d}{d\omega}\ln|R(\omega)|\,d\omega \tag{2.11}$$

Dispersion relations of this type require knowledge of the integrand over the entire spectral range. Experiments always fall short of this requirement and proper extrapolations must be applied beyond the range of measurement. However, in modulated reflectance spectra, the *Kramers-Kronig* relations are replaced by dispersion relations for the change in the optical constants generated by the modulation. The integrand is then typically restricted to a few narrow regions of the spectrum which reduces the consequences of an improper extrapolation.

To investigate the probability of an elementary absorption process in a semiconductor, one has to consider the perturbation caused by an electromagnetic field [4]. It stimulates the transition of an electron with initial energy E_i and wave vector $\bar{k}$ to a final state with energy E_f and wave vector $\bar{k}'$. When the electric field of frequency ω and polarization $\bar{e}$ is described as a time-dependent perturbation operator in the *Hamiltonian* of the system, the probability of finding the electron in the excited state is given by the matrix element of the perturbation. The number of transitions per unit time is

$$\frac{dN}{dt} \sim |\bar{e}\cdot M_{if}|^2 \cdot \delta(E_f - E_i - \hbar\omega) \tag{2.12}$$

where $\bar{e}\cdot M_{if}$ is the dipole matrix element of the perturbing light wave with respect to the wave function of the initial and final states

$$\bar{e}\cdot M_{if} = \int \psi_f^*(\bar{k}',\bar{r})\cdot\bar{e}\cdot\nabla\psi_i(\bar{k},\bar{r})\,d\bar{r} \tag{2.13}$$

The delta-function stipulates that no transitions can occur unless the photon energy matches the energy difference between initial and final states. This refers to the whole system because the transition may involve a complex many-body process. In order to draw conclusions about the one-electron states of the energy-band model, E_f and E_i must be assumed at the same values before and after the absorption, so that the creation of an electron-hole pair has no significant influence on the electronic states of the crystal. The coupling of the polarization vector $\bar{e}$ into the wave functions of initial and final states, imposes selection rules on the transition that depend on the symmetry character of these functions. Certain orientations of the polarization make the integral (2.13) vanish, meaning that the transition is not allowed.

In cubic crystals, the components x, y and z of the polarization vector $\bar{e}$ transforms in a manner that renders the selection rules independent of its direction. Therefore, polarization experiments do not give additional information over the same experiment performed with non-polarized light. Summation over equivalent directions in a cubic crystal averages out the anisotropies of the matrix element. In most modulated reflectance techniques a vectorial modulation parameter perturbs the symmetry of a cubic crystal, so that the anisotropies of the matrix element no longer average out. This can only be accomplished in static reflectance by *prestressing* the sample in some way.

The matrix element can be simplified if only wave functions of the *Bloch*-type are admitted

$$\psi = \exp[i\bar{k} \cdot \bar{r}] \cdot u(\bar{k}, \bar{r}) \tag{2.14}$$

and the incident light is assumed to be a plane wave. The concept of the direct transition then follows. The matrix element is zero unless the condition

$$\bar{k} - \bar{k}' + \bar{q} = \bar{0} \tag{2.15}$$

is fulfilled, where $\bar{q}$ is the momentum of the absorbed photon. Since, in the optical range, this momentum is always small on the scale of the first *Brillouin* zone (BZ) and therefore small compared to $\bar{k}$ and $\bar{k}'$, it is usually ignored. This means that the absorption process connects states that are located vertically above each other in the conventional $(E, \bar{k})$ diagram of the band structure.

2.1.3 The Joint Density-of-States Function

A correlation between ϵ_2 and the band stucture can be established assuming that absorption is the sum of transitions between electronic states of the same $\bar{k}$-vector (according to 2.15) and separated by the energy difference $E_f - E_i = \Delta E = \hbar\omega$ [4],

$$\epsilon_2(\omega) \sim \int_{BZ} \frac{2}{(2\pi)^3} \cdot |\bar{e} \cdot M_{if}|^2 \cdot \delta(\Delta E - \hbar\omega)\, d^3k \tag{2.16}$$

If we further assume that the matrix element is the same for all pairs of states located vertically above each other, regardless of their location in the BZ, we can define the joint density-of-states function $J(\Delta E)$ as

$$J(\Delta E) = \int_{BZ} \frac{2}{(2\pi)^3} \delta(\Delta E - \hbar\omega)\, d^3k \tag{2.17}$$

This simple counting of states in the BZ is the working hypothesis of band structure analysis. Therefore, ignoring the energy dependence of the matrix element:

$$\epsilon_2(\omega) \sim J(\Delta E)|\bar{e} \cdot M_{if}|^2. \tag{2.18}$$

A transformation of the volume integral in (2.17) into a surface integral over the surface $\Delta E = constant$ shows the properties of the joint density-of-states function more clearly. This transformation gives

$$J(\Delta E) = \frac{2}{(2\pi)^3} \int_{\Delta E = const} \frac{ds}{|\nabla_k(\Delta E)|} \tag{2.19}$$

where ds is the surface element on the isoenergetic surface $\Delta E = constant$ and $\nabla_k(\Delta E)$ is the gradient of the separation of initial and final states in k-space.

2.1.4 Critical Points on the Isoenergetic Surface

Points for which $\nabla_k(\Delta E) = 0$ are particularly important [4]. The gradients of the lines $E_f(k)$ and $E_i(k)$ are equal, and the density of states is large, since their separation does not change over a small region of $\bar{k}$-space. In such a point, known as a critical point, the denominator of the integrand in (2.18) is zero, and the joint density-of- states function passes through a slope discontinuity.

This condition on $E_f(k)$ and $E_i(k)$ can be satisfied in two different ways. First, the lines $E_f(k)$ and $E_i(k)$ can be parallel, but not horizontal. This can occur anywhere in the BZ, and such a critical point is therefore called a "general" critical point. Secondly, both $\nabla_k E_f$ and $\nabla_k E_i$ can vanish separately if the gradients are horizontal. Critical points of this kind can occur as a consequence of the periodicity of the $E(\bar{k})$ functions, in which case their position in $\bar{k}$-space is predictable from symmetry alone. This is a necessary condition at the center and the edges of the BZ for reasons of symmetry and the multiple connection of the zone. Such a critical point is called a "symmetry" critical point.

Since critical points are present at points of high symmetry in the BZ, the following working hypothesis of band structure analysis can be formulated.

1. Critical points introduce slope discontinuities into the joint-density- of-states function and into ϵ_2. They correlate to the band separation at points of high symmetry in the BZ, such as the center or edges.

2. Critical points can be classified into four different groups by developing $\Delta E = E_f - E_i$ into a *Taylor* series

$$\Delta E = \Delta E_0 + \sum_{\alpha=1}^{3} a_\alpha (k_\alpha - k_0)^2 \tag{2.20}$$

around the critical point at $\bar{k_0}$. The band separation can either be at an extremum in $\bar{k_0}$, in which case all α_i are positive (minimum) or negative (maximum). Since ΔE increases (decreases) in all directions of $\bar{k}$-space, the critical point is called "parabolic".

3. ΔE can on the other hand , increase in two (one) of the principal directions selected for the coordinate system in (2.19). One (two) of the $\alpha's$ is negative, and a critical point of this type is called a "hyperbolic" or "saddlepoint" critical point. It should be noted that there is a characteristic line shape for each critical point, which gives a valuable tool for identifying the structure in optical spectra which are experimentally observed.

4. Modulation of the spectral position E_g of a critical point affects ϵ_2 through the joint density-of-states function, $J(E_g, \hbar\omega)$,

$$\frac{\Delta\epsilon_2}{\Delta E_g} = \frac{C}{\omega^2} \cdot \frac{\Delta J}{\Delta E_g} \tag{2.21}$$

where C contains the matrix element and effective mass parameters. At all four types of critical points, the joint density-of-states function varies as the square root of the spectral distance from E_g. Hence, the derivative with respect to E_g has a singularity of the type $(E_g - \hbar\omega)^{-1/2}$ at the critical point. This singularity at critical points probably explains the spectral selectivity of modulated reflectance. The response disappears as the spectral distance from the critical point increases. Noncritical areas in which the joint density-of-states function is smooth and free of square-root slope discontinuities should not be affected by the modulation.

The modulation of ϵ_2 is transferred to ϵ_1 through a differential *Kramers-Kronig* relation

$$\Delta\epsilon_1(\omega_0) = \frac{2}{\pi}\int_0^\infty \frac{\omega \cdot \Delta\epsilon_2(\omega)}{\omega_0^2 - \omega^2}\, d\omega \tag{2.22}$$

which is easily derived from (2.8) by using $\epsilon_2' = \epsilon_2 + \Delta\epsilon_2$ under the integral and subtracting. Contributions to the integral in (2.21) are restricted to the spectral regions in which the modulation affects ϵ_2. This is of considerable practical value, since extrapolation outside the region of measurement is less critical. The transformation properties of the differential *Kramers-Kronig* relation is illustrated by again using the simple model of a modulation of E_g. In analogy to (2.20)

$$\frac{\Delta\epsilon_1}{\Delta E_g} = \frac{2C}{\pi}\int_0^\infty \frac{\Delta J/\Delta E_g}{\omega(\omega_0^2 - \omega^2)}\, d\omega \tag{2.23}$$

The relation between $\Delta\epsilon_1$ and $\Delta\epsilon_2$ for a given critical point, as well as the relation between $\Delta\epsilon_1$ or $\Delta\epsilon_2$ at two different types of critical points, is independent of the choice of mechanism and reflect the transformation properties of the differential *Kramers-Kronig* relation. It is not realistic to assume that the electron stays in the excited state indefinitely. It will leave through recombination or interaction with another electron or phonon. As a consequence

of the uncertainty principle, this limited lifetime in the excited state leads to a broadening of initial and final states. By using the phenomenological *Lorentzian* broadening parameter Γ, the effect of this lifetime broadening on ϵ_2 is described by the convolution

$$\epsilon_2(\omega)_{LB} = \int_0^\infty \frac{\Gamma \cdot \epsilon_2(\omega')}{(\omega - \omega')^2 + \Gamma^2} \, d\omega'. \tag{2.24}$$

2.2 Electromodulation Lineshapes

2.2.1 Qualitative Discussion

The objective of modulation spectroscopy is to obtain sharp, well resolved spectra that can be analyzed to directly yield the properties of the material under study [6]. However, PR spectra in general are strongly dependent on the magnitude of the applied field and on experimental conditions so that the determination of material parameters from these spectra is a difficult and uncertain process. However, at sufficiently low values of the modulating electric field, PR spectra simplify drastically. As with all modulation techniques, the perturbation (the electric field, $\bar{F}$) changes with the dielectric properties of the unperturbed solid. These changes are described in terms of a change, $\Delta\epsilon(\bar{F})$, of the complex dielectric function ϵ. The quantity $\Delta\epsilon(\bar{F})$ is obtained by adding a perturbation term, H' to the *Hamiltonian* H_0 of the unperturbed crystal. For a uniform electric field, $H' = e\bar{F} \cdot \bar{r}$. It is of fundamental importance that, in contrast to other forms of modulation spectroscopy (such as piezoreflectance, thermoreflectance or wavelength modulation), the perturbation term $e\bar{F} \cdot \bar{r}$ for the electric field is not lattice-periodic: it represents a net force that accelerates the electron, and it therefore completely destroys the translational invariance of the Hamiltonian in the field direction. Although this appears to be a trivial property of the field perturbation, it is in fact the central reason for the complexity of PR theory. It also accounts for the remarkable relationship between low-field PR spectra and the third-derivative of the unperturbed dielectric function, which stands in direct contrast to mod-

ulation techniques where lattice periodicity is retained and first-derivative spectra are observed. The fundamental importance of translational invariance in determining dielectric properties in general, can be seen from a simple physical model. For a free electron, the *Hamiltonian*, $H_0 = p^2/2m$, is invariant to any translation and therefore the electron momentum, $\bar{p} = \hbar\bar{k}$, is rigorously conserved. Here, the energy band structure is simply a parabola, $E = \hbar^2k^2/2m$. A photon cannot be absorbed to first order in this system because its momentum is negligibly small and its energy, $E = \hbar\omega$, if absorbed by the electron, would involve a relatively large momentum change. Thus, energy and momentum cannot both be conserved in a first-order optical transition. It follows that the sum of all allowed transitions for any finite photon energy (i.e., the imaginary part, ϵ_2, of the complex dielectric function, $\epsilon = \epsilon_1 + \epsilon_2$) is identically zero for the free electron. If the electron is in a crystal, the *Hamiltonian*, $H_0 = p^2/2m + V(\bar{r})$, is now invariant only to the class of translations that takes the crystal into itself. Momentum conservation is weakened, and the momentum $\hbar\bar{k}$ is now a good quantum number only to within a vector, $\bar{K}_n$, of the reciprocal lattice. The free-electron energy parabola breaks up into energy bands and optical absorption is now possible in first order by utilizing a reciprocal lattice vector to obtain momentum conservation. In the reduced zone scheme, the optical transition will appear as a vertical line in an energy band structure diagram as indicated in the upper half of figure 2.2.

If the crystal is now perturbed, its *Hamiltonian*, $H_0 = p^2/2m + V(\bar{r}) + H'$, will generally have lower symmetry depending on the form of H'. If periodicity is retained, as for example in piezoreflectance, momentum is still a good quantum number to within the reciprocal lattice vector. Optical transitions remain vertical and the dominant changes appear directly as small shifts in energy gaps or amplitudes of momentum matrix elements. Since these shifts are generally small on the scale of energy gaps, the perturbation induced changes in ϵ are of first order and are approximated by first-derivative lineshapes. If the perturbation is an electric field, $H' = e\bar{F} \cdot \bar{r}$, translational invariance is lost, the electron is accelerated and momentum is no longer a good quantum

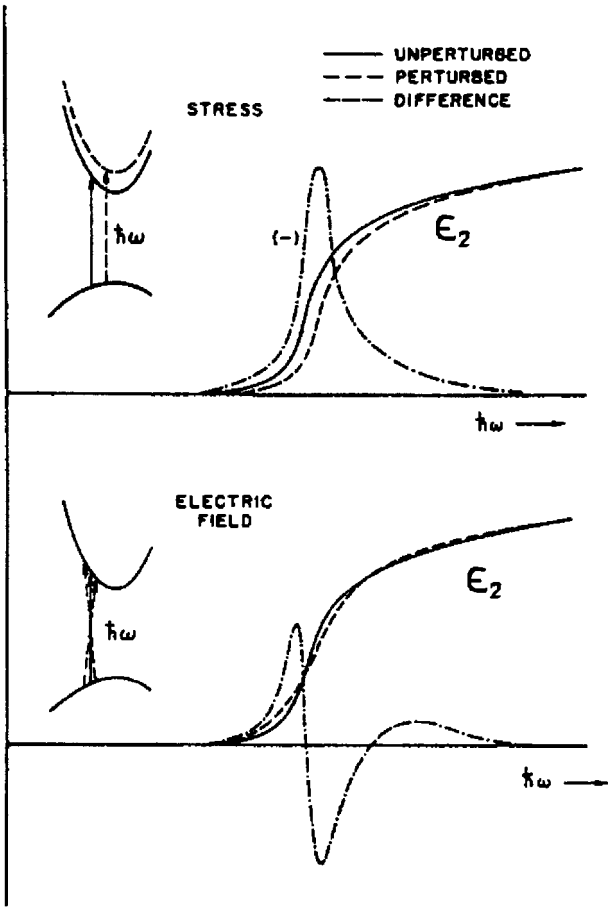

Figure 2.2: Schematic diagram of the change in the imaginary part of the dielectric function.

number in the field direction. Consequently, the one-electron *Bloch* functions of the unperturbed crystal become mixed. This is equivalent to spreading the formerly sharp vertical transitions over a finite range of initial and final momenta, as shown at the bottom of figure 2.2. In the case of small fields, mixing will be restricted to those wavefunctions near the originally vertical allowed transition. This will yield a complicated difference spectrum having changes in sign as indicated in the bottom half of figure 2.2. The two zero crossings are characterictic of the third-derivative, as may be verified qualitatively by explicit calculation. Alternatively, it might be anticipated that the averaging effect of the momentum-space mixing of wave functions in the case of electric field perturbations, would lead to effective energy shifts analogous to those encountered in periodicity-retaining perturbations, except for being much "smoother" functions (*i.e.*, higher-order) of the perturbation, thus resulting in higher-order changes in ϵ (*i.e.*, higher-derivative-spectra). To prove this statement, consider the time dependence of the average energy of a band electron in a perturbation turned on instantaneously at $t = 0$. If periodicity is preserved, the perturbation simply produces a discontinuous change in the zero-order (constant) terms (E_g or Γ) in a *Taylor* series expansion of the average energy as a function of time. In the case of an electric field, the discontinuity occurs in the acceleration, which appears in the second-order, or quadratic term in the time-dependent average energy. Thus, no discontinuities occur either in E_g or in the initial momentum at $t = 0$ for the electric field perturbation. If a transformation into the frequency domain is made to calculate ϵ, it is found that a small discontinuity in the zero-order terms, E_g and Γ, leads to a first-order change in ϵ (first-derivative spectrum). Similarly, a small discontinuity in the second-order term, leads to a third-order change in ϵ (third-derivative spectrum).

2.2.2 Theoretical Description

For the case of bulk materials with an applied electric field, the main effect of the electric field is to change the wave vector of the *Bloch* state from $\bar{k}$ to $\bar{k} + e\bar{F}t/\hbar$, where $\bar{F}$ is the applied electric field [1]. Mathematically, this sub-

stitution expresses the fact that the field mixes all wave functions that have components along the field direction. The magnitude of the mixing is determined by the time parameter, t. From a free particle point of view, the electron or hole is driven up its dispersion curve and its energy is changed continuously, giving the appearance that it is accelerated in the electric field. For the purpose of this discussion, the most useful expression for the dielectric function involves the *Fourier* transform of the time-dependent current. The general expression for ϵ is

$$\begin{aligned}\epsilon(E,\Gamma) &= 1+\frac{4\pi i e^2\hbar}{m^2E^2}\int_{BZ}d^3k\int_0^\infty dt|\bar{e}\cdot\bar{p}_{cv}|^2 \\ &\quad\times\exp\left[\int_{-t/2}^{t/2}dt'\,\frac{i[E-E_{cv}(\bar{k})+i\Gamma]t'}{\hbar}\right] \qquad (2.25)\end{aligned}$$

where Γ is a phenomenological Lorentzian lifetime broadening parameter, defined in (2.24), $\bar{p}_{cv}$ is the momentum matrix element between the conduction and the valence band, E_{cv} is the energy difference between the conduction and the valence band, and E is the photon energy [5]. Replacing $\bar{k}$ with $\bar{k}+e\bar{F}t/\hbar$ in E_{cv} of (2.25) and expanding in a *Taylor* series around $\bar{k}$, one gets

$$\epsilon(E,F,\Gamma)=1+\frac{iA}{E^2}\int_{BZ}d^3k\int_0^\infty dt\exp\left[\frac{i(E-E_{cv}+i\Gamma)t+i\Omega t^3/3}{\hbar}\right] \qquad (2.26)$$

where $\Omega^3=e^2F^2/8\mu\hbar$, $A=4\pi E^2\hbar|\bar{e}\cdot\bar{P}_{cv}|^2/m^2$, and μ is the joint density-of-states effective mass in the direction of the applied electric field. Equation (2.25) is the general expression for an *Airy* function.

A simplification occurs when the field is small or when the homogeneous broadening is large; *i.e*, $\Gamma t \gg \Omega t^3$. Expanding the exponent containing $\Omega[\exp(i\Omega t^3/3) \approx 1 + i\Omega t^3/3]$ leads to the small-field limit

$$\epsilon(E,F,\Gamma) = 1 + \frac{iA}{E^2}\int_{BZ} d^3k \int_0^\infty dt \left(1 + \frac{i\Omega t^3}{3\hbar}\right) \exp\left[\frac{i(E - E_{cv} + i\Gamma)t}{\hbar}\right] \tag{2.27}$$

In (2.27) the term in the square brackets represents the unperturbed dielectric function and the term in brackets represents the field-dependent perturbation. The time dependence (t^3) of the perturbation term can be obtained by differentiating the unperturbed term under the integral three times with respect to E (and also Γ) or E_{cv}. Integrating (2.27) yields the final form

$$\begin{aligned}\epsilon(E,F,\Gamma) &= 1 + \frac{iA}{E^2}\int_{BZ} d^3k \frac{1}{E - E_{cv} + i\Gamma} \\ &\quad + \frac{2iA}{E^2}\int_{BZ} d^3k \frac{(\hbar\Omega)^3}{(E - E_{cv} + i\Gamma)^4}\end{aligned} \tag{2.28}$$

This result is known as the *Aspnes* third-derivative functional form. The term in t^3 arises directly from the fact that there is a dispersion curve along the field direction and hence a gradient with respect to $\bar{k}$. This result is particularly significant, from a spectroscopic point of view, because third-derivative lineshapes are characterized by the presence of strongly enhanced critical point structures and strongly supressed background effects. The widths of these third-derivative critical point structures are determined by lifetime broadening. These spectral features are well localized in energy, allowing nearly degenerate critical points to be resolved. Moreover, this localization permits the actual energy band structure in the vicinity of critical points to be approximated accurately by simple model densities of states, enabling critical point energies and broadening parameters to be obtained directly and precisely from experimental data without requiring either a separate measurement of the optical constants or data reduction by *Kramers-Kronig* analysis. A simple physcial derivation of the effects of a small electric field on the dielectric function will be given [8]. The energy gained by a free particle in an electric field is calculated first. This is done by replacing $\bar{k}$ with $\bar{k} + e\bar{F}t/\hbar$ to obtain

[4]:

$$E = e^2F^2t^2/2\mu \tag{2.29}$$

where t is the time and μ is the joint density-of-states effective mass in the direction of the applied electric field $\bar{F}$. Considering an optical structure near a critical point, with energy E_g, the dielectric function has the general form:

$$\epsilon = \epsilon(E - E_g, \Gamma) \tag{2.30}$$

where E is the photon energy. The electric field induced change in the dielectric function, $\Delta\epsilon$, is given by:

$$\Delta\epsilon = \epsilon[E - E_g + E(F)] - \epsilon[E - E_g] \tag{2.31}$$

If the field is sufficiently small, so that $E(F) \ll \Gamma$ (low field regime), (2.31) can be expanded into a Taylor series to yield:

$$\begin{aligned} \Delta\epsilon &= E(F)(d/dE)\epsilon(E - E_g, \Gamma) \\ &= (e^2F^2t^2/2\mu)(d/dE)\epsilon(E - E_g, \Gamma) \end{aligned} \tag{2.32}$$

Taking into account that, in quantum mechanics, the time t is an operator,

$$t = i\hbar(d/dE) \tag{2.33}$$

(2.32) becomes:

$$\Delta\epsilon = (e^2F^2\hbar^2/2\mu)(d^3/dE^3)\epsilon(E - E_g, \Gamma) \tag{2.34}$$

$$= 4(\hbar\Omega)^3(d^3/dE^3)\epsilon(E - E_g, \Gamma) \tag{2.35}$$

where the electro-optic energy $(\hbar\Omega)^3$ is given by:

$$(\hbar\Omega)^3 = e^2F^2\hbar^2/8\mu \tag{2.36}$$

Equation (2.36) has all of the essential features of low-field electro-modulation (EM). The quantity $\Delta\epsilon$ is proportional to F^2 (modulating field), inversely proportional to μ and has a line shape that is the third-derivative of the unperturbed optical function. The following section will be devoted to the evaluation of the dielectric function and the critical point types, as it will aid in the determination of the band structure parameters.

2.2.3 The Dielectric Function and Critical Point Types

In section 2.2.1 the physical origin of the third-derivative behaviour of low-field electro-reflectance (ER) spectra was discussed in terms of a simple model, emphasizing the crucial part played by translational symmetry in this effect. In this section the field-induced change in the dielectric function, $\Delta\epsilon$, is discussed in terms of perturbation theory. The loss of translational invariance due to an electric field, results in the appearance of a second, intraband, or one-band acceleration mechanism that substantially modifies the phase-coherent or long-range correlation part, $e^{i\bar{k}\cdot\bar{r}}$, of the unperturbed *Bloch* functions, $|n,\bar{k}\rangle = e^{i\bar{k}\cdot\bar{r}}u_n(\bar{k},\bar{r})$. The existence of the usual interband mechanism acting on the periodic part, $u_n(\bar{k},\bar{r})$, of the *Bloch* functions, is easily demonstrated by imagining that the linearly increasing potential of the uniform field consists of two parts, namely a sawtooth component having lattice periodicity, and a staircase component describing the loss of translational invariance [9]. The sawtooth component results in *Stark* shifts of the energy bands and momentum matrix element changes which lead to first-derivative contributions to ER spectra. When the externally applied fields are such that both intraband and interband mechanisms can be treated adequately by first-order perturbation theory, low-field ER spectra are observed. Perturbation theory implies that the perturbation itself has a certain characteristic energy and at the same time, the system being perturbed also has a characteristic energy. The perturbation and system energies for the interband mechanism in ER, are $e\mathcal{E}a_0$, the potential drop across the unit cell, and E_g, the energy separation between the pair of bands under consideration [10] ($\mathcal{E}$ and a_0 represent the perturbing field and the interatomic spacing respectively). For the interband mechanism, perturbation theory will apply whenever $e\mathcal{E}a_0 \ll E_g$. In the case of the intraband mechanism, the characteristic energy for the system is Γ, the broadening parameter, whereas the perturbation energy is given by [6]:

$$\hbar\Omega = (e^2\mathcal{E}^2\hbar^2/8\mu)^{\frac{1}{3}} \tag{2.37}$$

$$= [e^2(\mathcal{E}\cdot\nabla_{\bar{k}})^2 E_{cv}(\bar{k})/8]^{\frac{1}{3}}, \tag{2.38}$$

where μ is the effective mass of the conduction and valence bands, evaluated in the field direction, and $E_{cv}(\bar{k})$ is the interband energy at $\bar{k}$. Equation (2.38) is derived from (2.37) using the relation [9]

$$\mu = \frac{\hbar^2}{\nabla^2_{\bar{k}} E_{cv}} \tag{2.39}$$

The energy $\hbar\Omega$ is of course the electro-optic energy, obtained in the quantum mechanical solution of a particle with effective mass μ, which is accelerated in a uniform field. Perturbation theory will apply to the intraband mechanism whenever $|\hbar\Omega| \ll \Gamma$. It would be useful to attach a physical meaning to the energies $\hbar\Omega$ and Γ for the intraband mechanism. This is done by calculating the average energy per particle, $\langle\Delta W\rangle$, absorbed in a collision period, τ, for a collection of classical particles of charge $-e$, mass μ, and zero average initial velocity (zero initial current) being accelerated in a uniform field, $\mathcal{E}$. It is known that $dW = \bar{F}\cdot\bar{v}(t)dt$, ($\bar{F}$ representing the force on a particle) where $\bar{F} = -e\mathcal{E}$ and $\bar{v}(t) = \bar{v}_0 + \bar{a}t = \bar{v}_0 - (e\mathcal{E}/\mu)t$, and consequently

$$\langle\Delta W\rangle \sim \left\{\int_0^\tau dt(-e\mathcal{E})\cdot[\bar{v}_0 - (e\mathcal{E}/\mu)t]\right\} = e^2\mathcal{E}^2\tau^2/(2\mu). \tag{2.40}$$

The lifetime, τ, is related to the broadening energy, Γ, by $\tau \sim \hbar/(2\Gamma)$. If $\langle\Delta W\rangle$ is interpreted as a field-induced uncertainty in the unperturbed electron energies, analogous to the interpretation of Γ as a lifetime-induced uncertainty in these levels, then $\langle\Delta W\rangle/\Gamma \sim (e^2\mathcal{E}^2\hbar^2/8\mu\Gamma^3) = (\hbar\Omega/\Gamma)^3$. Therefore, perturbation theory applies to the intraband mechanism whenever the average energy gained per particle, due to the acceleration caused by the electric field, is small compared to the natural lifetime-induced uncertainty in the unperturbed electron energy levels. First-order perturbation theory is known to be a good approximation only if the perturbation energy is appreciably less than the characteristic system energy[6], and it is therefore evident that the intraband mechanism will determine the low-field limit. The high-field limit occurs when $e\mathcal{E}a_0 \sim E_g$, and corresponds to the breakdown of selection rules, Stark shifts of energy bands, and first-derivative contributions to ER spectra

similar to those obtained with other modulation techniques. However, at these fields the intraband contribution usually dominates, so high-field spectra are usually important only very near points of degeneracy. The interband mechanism can be neglected for both the intermediate and low-field ranges. For a single band pair c, v the intermediate-field-expression for $\Delta\epsilon$, in terms of a general energy band structure defined by $E_{cv}(\bar{k})$ [6], is

$$\begin{aligned}\Delta\epsilon^{ij}(\mathcal{E},\Gamma,E) &\cong \frac{4\pi i e^2\hbar^2 P^i_{vc}P^j_{cv}}{m^2E^2}\left(\frac{2}{(2\pi)^3}\right)\int_{BZ} d^3k \int_0^\infty ds e^{-\Gamma s}e^{iEs} \\ &\times\left\{\exp\left[-i\int_{-s/2}^{s/2} ds' E_{cv}(\bar{k}-e\mathcal{E}s')\right]\right. \\ &\left.-\exp\left[-iE_{cv}(\bar{k})s\right]\right\} \qquad (2.41)\\ &\cong \frac{4\pi i e^2\hbar^2 P^i_{vc}P^j_{cv}}{m^2E^2}\left(\frac{2}{(2\pi)^3}\right)\int_{BZ} d^3k \int_0^\infty ds\, e^{-\Gamma s} \\ &\times \exp[i(E-E_{cv}(\bar{k}))s]exp[-i(\hbar\Omega(\bar{k}))^3s^3/3]-1 \qquad (2.42)\end{aligned}$$

In (2.41), the momentum matrix elements are assumed to be independent of $\bar{k}$ and also, the energy bands are assumed to be locally parabolic, which then leads to (2.42). If in addition the energy bands are assumed to be completely parabolic, (2.42) can be expressed in closed form and the *Franz-Keldysh* expression is obtained. Lastly, the intermediate field range is identified experimentally by the complex line-shape dependence on the field, the appearance of subsidiary oscillations in ER spectra, and an exponential dependence of the fundamental absorption edge. The lifetime broadening term $e^{-\Gamma s}$ in (2.42) will cut of the integrand before the term, $exp[-i(\hbar\Omega)^3s^3/3] \cong 1-i(\hbar\Omega)^3s^3/3+...$, changes appreciably, provided that the field is sufficiently small ($(\hbar\Omega)^3 \sim \mathcal{E}^2$). Furthermore, if $|\hbar\Omega| < \Gamma/3$, it has been shown that the higher-order terms may be neglected. After explicit integration the low-field expressions are obtained:

$$\begin{aligned}\Delta\epsilon^{ij}(\mathcal{E},\Gamma,E) &\cong \frac{8\pi^2\hbar^2 P^i_{vc}P^j_{cv}}{m^2E^2}\left(\frac{2}{(2\pi)^2}\right)\int_{BZ} d^3k \frac{(\hbar\Omega)^3}{(E_{cv}(\bar{k}-E-i\Gamma)^4} \qquad (2.43)\\ &\cong \frac{(\hbar\Omega)^3}{3E^2}\frac{\partial^3}{\partial E^3}(E^2\epsilon^{ij}(\Gamma,E) \qquad (2.44)\end{aligned}$$

$$= \frac{e^2\hbar^2\mathcal{E}^k\mathcal{E}^l}{24E^2}(\mu^{-1})^{kl}\frac{\partial^3}{\partial E^3}(E^2\epsilon^{ij}(\Gamma, E) \tag{2.45}$$

The third-derivative relationship between the field-induced change, $\Delta\epsilon$, and the unperturbed dielectric function, ϵ is clearly evident in (2.44) and (2.45). Equation (2.45) also shows the experimentally identifying feature of low-field spectra, namely the quadratic scaling dependence of an invariant lineshape on an externally applied field.

The quantity $\Delta\epsilon$, given by (2.41) to (2.45) can be related to the experimentally observed relative change in reflectivity, $\Delta R/R$, by

$$\frac{\Delta R}{R} = Re[C_s C_{ex} C_{in} e^i e^j \Delta\epsilon^{ij}], \tag{2.46}$$

where

$$C_s = 2n_a/[n(\epsilon - \epsilon_a)], \tag{2.47}$$

$$C_{ex} = [1 - g(\epsilon - 1)]^2, \quad g \leq 0, \tag{2.48}$$

$$C_{in} = -2ik \int_{-\infty}^{0} dz'\, e^{-2ikz'}[\mathcal{E}(z')/\mathcal{E}(0)]^2 \tag{2.49}$$

and e^i and e^j represent Cartesian components of the unit polarization vector, $\hat{e}$, and g is a so-called strength parameter, which can be assumed to be constant for a given structure. The *Seraphin* coefficients[2], α and β, for a two-phase interface (ambient $n_a^2 = \epsilon_a$, unperturbed substrate $n^2 = \epsilon$) are given by the factor $C_s = \alpha - i\beta$, which is rewritten in complex-variable form for convenience. C_{ex} represents the electron-hole *Coulomb* interaction [12], and C_{in} is the factor arising from the spatial dependences, or inhomogeneities in the perturbing field [13].

2.2.4 Simple Parabolic Model for Densities of States

The energy band structure in the vicinity of a critical point can usually be accurately replaced with a simple parabolic model [6] which aid in the analysis of experimental spectra for band structure parameters. This can be ascribed to the fact that the low-field ER structure of a single critical point is strongly

localized to within an energy range not exceeding several broadening parameters. For one-, two-, and three-dimensional simple parabolic model densities of states (D = 1, 2, and 3 respectively), (2.43) becomes [4]

$$D = 1: \ \Delta\epsilon^{ij} = \left(\frac{5i^{l-1}}{8}\right)\left(\left|\frac{2\mu_x}{\hbar^2}\right|^{\frac{1}{2}} K_y K_z\right) \mathcal{Q}^{ij}\,\mathcal{E}^2\,(E - E_g + i\Gamma)^{-7/2}, \quad (2.50)$$

$$D = 2: \ \Delta\epsilon^{ij} = \left(\frac{2i^{l-2}}{3}\right)\left(\left|\frac{4\mu_x\mu_y}{\hbar^4}\right|^{\frac{1}{2}} K_z\right) \mathcal{Q}^{ij}\,\mathcal{E}^2\,(E - E_g + i\Gamma)^{-3}, \quad (2.51)$$

$$D = 3: \ \Delta\epsilon^{ij} = \left(\frac{\pi i^{l-3}}{4}\right)\left(\left|\frac{8\mu_x\mu_y\mu_z}{\hbar^6}\right|^{\frac{1}{2}}\right) \mathcal{Q}^{ij}\,\mathcal{E}^2\,(E - E_g + i\Gamma)^{-5/2}, \quad (2.52)$$

where

$$\mathcal{Q}^{ij} = \frac{e^4\hbar^4 P_{vc}^i P_{cv}^j}{8\pi\mu_{||}E^2 m^2}; \quad (2.53)$$

l is the order of the critical point, equal to the number of negative effective masses μ_x, μ_y, μ_z; K_y and K_z represent k space cutoff limits used for $D = 1$ or $D = 2$; $\mu_{||}$ is the interband reduced mass evaluated in the field direction as defined in (2.37) and (2.38). In the described model, the energy location of $\Delta\epsilon^{ij}$ is determined by the band gap, E_g, its width by the broadening parameter, Γ, its amplitude by a combination of Γ, the momentum matrix elements $\bar{P}_{cv}$, the electric field $\mathcal{E}$, and the effective masses μ_i, and finally the general lineshape is determined by the complex phase factors together with the sign of $\mu_{||}$. It should be noted that in this model the field $\mathcal{E}^2$ only interacts with the parameters determining the amplitude. Therefore, Γ, E_g, and the phase factor can be determined from an experimentally determined spectrum $\Delta\epsilon$ without requiring the value of $\mathcal{E}$. Equations (2.47) to (2.49) describes the three major interactions that take $\Delta\epsilon$ into the experimentally measured lineshape $\Delta R/R$, namely the optical properties of the ambient and the material, the electron-hole correlation effects, and the field inhomogeneities.

In general, experimental ER spectra exhibit a relatively simple line shape which has both positive and negative extrema. These experimental line-

shapes are approximated by a perturbation treatment of ER [16], which describe the modulated reflectivity spectra $\Delta R/R$ as

$$\frac{\Delta R}{R} = Re(Ce^{i\theta}\Delta\epsilon). \tag{2.54}$$

The field-induce change in the dielectric function, $\Delta\epsilon$, has the resonant form

$$\Delta\epsilon \sim (E_g - \hbar\omega - i\Gamma)^{-n}, \quad n \geq 2. \tag{2.55}$$

Aspnes and *Rowe* [15] determined that a least-squares fit to the experimental lineshape is sufficient to determine interband energies to high accuracy. They proposed a simple three-point fit of theory to experiment. The so-called three-point ratio ρ is defined as

$$\rho = -\left(\frac{\Delta R}{R_B}\right)\left(\frac{R_A}{\Delta R}\right) \tag{2.56}$$

where A and B are the *lower-* and *higher*-energy dominant peaks, respectively, of the $\Delta R/R$ spectrum. The position of E_g with respect to the energy E_A of peak A is given uniquely in terms of ρ:

$$E_g = E_A + \Delta E f(\rho), \tag{2.57}$$

where

$$\Delta E = E_B - E_A, \tag{2.58}$$

and f is the scaling parameter. The scaling parameter is plotted in figure 2.3 for three different values of n in (2.55). The value $n = 3$, corresponding to a two-dimensional critical point [15] is a good description of three-dimensional critical points with large mass ratios [17] [18] and fundamental absorption edges modified by the Coulomb interaction [19]. The values $n = 2$ and 2.5 describe the modulation of discrete excitons and general three-dimensional critical points, respectively [15]. Since the curves for all three values of n are nearly the same, it is evident that the three-point method is nearly independent of the physical model chosen to represent the transition.

This implies that the critical point energies and broadening parameters can be determined directly from the experimental $\Delta R/R$ lineshape, without

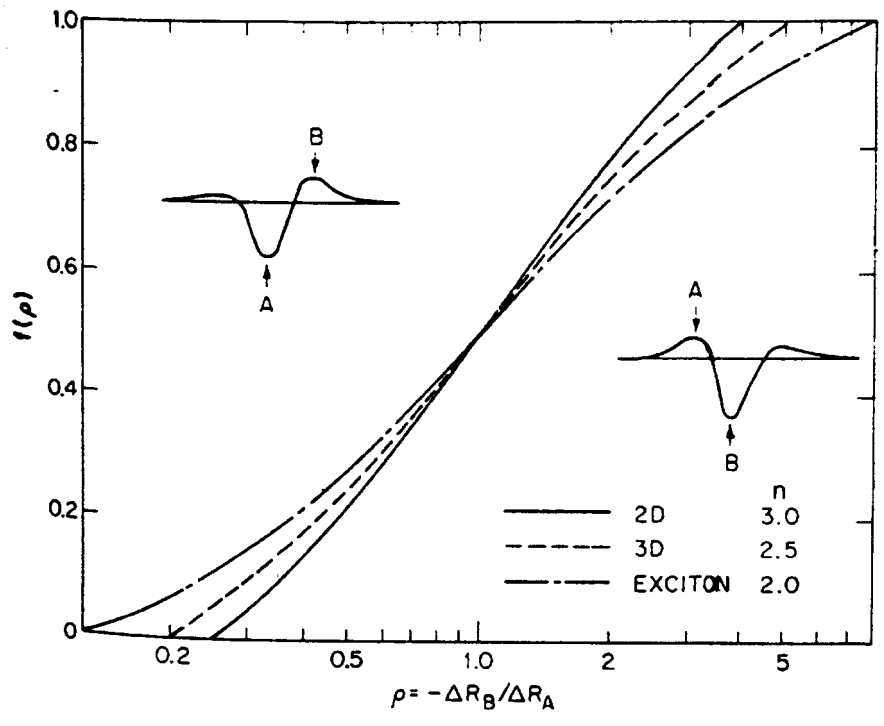

Figure 2.3: The scaling parameter plotted for three different values of n.

resorting to a *Kramers-Kronig* analysis, or a knowledge of the field inhomogeneity, electron-hole interaction strength, or even the optical properties of the material [14] [15]. Further spectroscopic information is contained in the phase and amplitude factors, but these depend on an interrelationship among the various mechanisms mentioned above, and the study of any one of these mechanisms in particular requires estimates of the phase and amplitude contributions from the others. Therefore, the entire analysis of an experimental spectrum in the simple parabolic model density of states approximation can be carried out in the framework of the experimental spectrum, $\Delta R/R$, because analysis of the data by means of a *Kramers-Kronig* analysis will provide no further information. If the dielectric function is varying rapidly in energy near a critical point structure, however, a *Kramers-Kronig* analysis is usually required.

2.2.5 Determination of Band Structure Parameters

PR spectra in general, and low-field spectra in particular, exhibit one positive and one negative extremum for each critical point. This is a general property of complex resonance lineshapes of the form

$$\frac{\Delta R}{R} = Re[Ce^{i\theta}(E - E_g + i\Gamma)^{-n}] \tag{2.59}$$

where C and θ are amplitude and phase factors that vary slowly with E and n [6]. The amplitude and phase factors C and θ determine the amplitude and asymmetry of the lineshape respectively, and E_g and Γ determine the energy location and width of the structure. The parameter n represents the type of critical point and order of the derivative.

Figure 2.4 shows how the parameters interact in determining the lineshape for the two-dimensional ($n = 3$) and three-dimensional ($n = 5/2$) simple parabolic critical point models. The amplitude factor only scales the lineshape determined by θ, n, E_g and Γ and thus does not enter into the actual lineshape determination. The phase, θ, is the dominant factor determining the lineshape, however, regardless of the value of θ, the energy gap always lie between the two extrema and the energy seperation between the two extrema is nearly constant. This suggests that E_g and Γ should be obtainable in a relatively straightforward manner from these lineshapes.

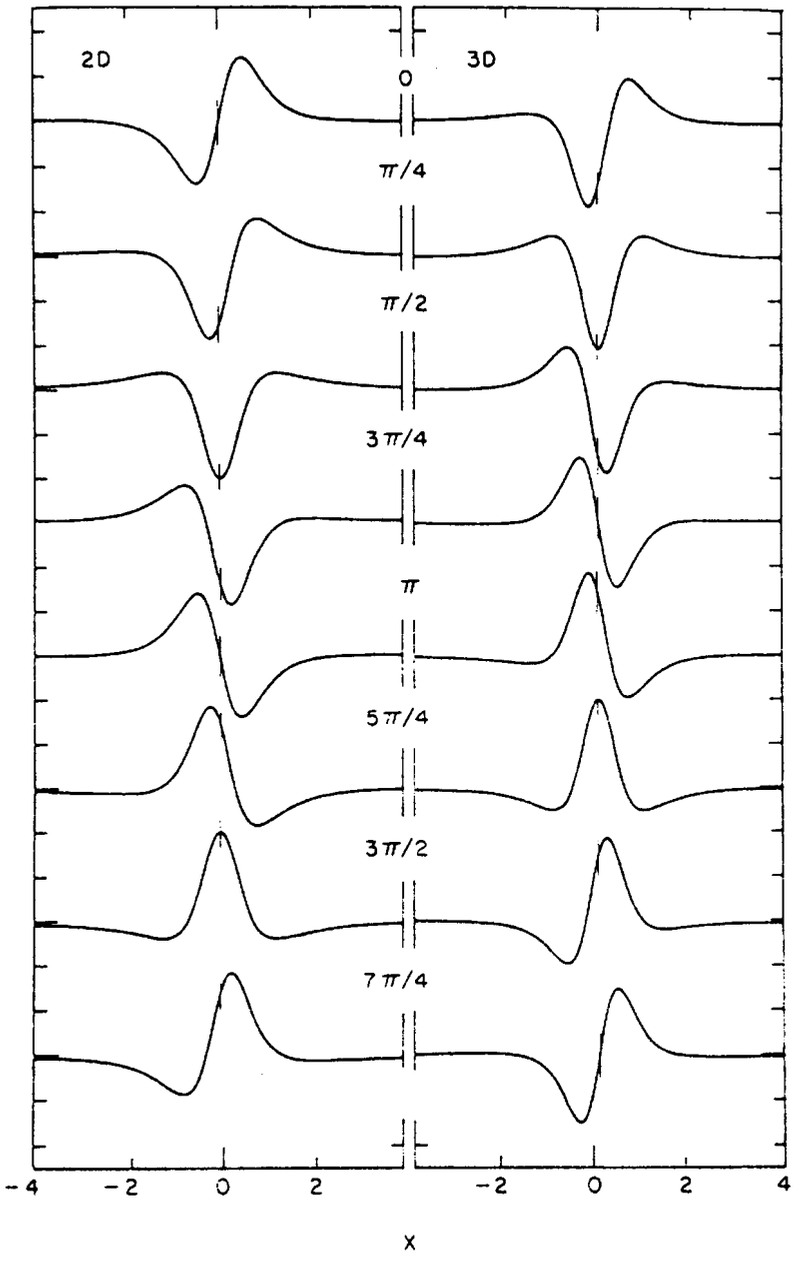

Figure 2.4: Variation of the lineshape $\Delta R/R$ with phase θ.

References

[1] Glembocki O.J., Shanabrook B.V. in *The Spectroscopy of Semiconductors : SEMICONDUCTORS AND SEMIMETALS* Vol. 36 Chapter 4

[2] Seraphin B.O., Bottka N., Phys. Rev. **145**, (1966), p.628

[3] Lipsanen H.K., Airaksinen V.M., Appl. Phys. Lett. **63**(21), (1993), p.2863

[4] Seraphin B.O. in *Modulated Reflectance : Optical Properties of Solids* p.163, edited by F. Abelès

[5] Aspnes D.E., Studna A.A., Phys. Rev. B **7** (10), (1973), p.4605

[6] Aspnes D.E., Surf. Sci. **37**, (1973), p.418

[7] Aspnes D.E., Row J.E., Phys. Rev. B **5**, (1972), p.4022

[8] Pollak F.H., Glembocki O.J., SPIE Vol. 946: Spectroscopic Characterization Techniques for Semiconductor Technology III p. 2, (1988)

[9] Enderlein R., Keiper R., Tausenfreund W., Phys. Status Solidi **33**, (1969), p.69

[10] Bottka N., Fischer J.E., Phys. Rev. B **3**, (1971), p.2514

[11] Blakemore J.S., Solid State Physics, Second Edition, (1974), p.238

[12] Rowe J.E., Aspnes D.E., Phys. Rev. Lett. **25**, (1970) p. 162

[13] Aspnes D.E., Frova A., Solid State Commun. **7**, (1969), p. 155

[14] Aspnes D.E., Rowe J.E., Bull. Am. Phys. Soc. **16**, (1971), p. 396

[15] Aspnes D.E., Rowe J.E., Phys. Rev. Lett. **27**, (1971), p. 188

[16] Aspnes D.E., Rowe J.E., Solid State Commun. **8**, (1970), p. 1145

[17] Kane E.O., Phys. Rev. **180**, (1969), p. 852

[18] Higgenbotham C.W., Cardona M., Pollak F.H., Phys. Rev. **184**, (1969), p. 821

[19] Elliott R.J., Phys. Rev. **108**, (1957), p. 1384

Chapter 3

Doping Superlattices

3.1 Introduction

In general there are two different types of superlattices, namely, compositional and doping superlattices. These artificially structured materials consist of a periodic sequence of ultrathin layers which have alternating composition or doping. A crystal which is made by depositing alternate layers of two different semiconductors, for example gallium arsenide and aluminium arsenide, is known as a compositional superlattice. When donor and acceptor impurities are incorporated into alternate layers of a single semiconducting material, for example n-doped and p-doped GaAs, it is known as a doping superlattice. In some cases the n- and p-doped layers are separated by undoped or intrinsic (i) layers of the same semiconductor, and therefore these doping superlattices are often referred to as *n-i-p-i* crystals. Doping superlattices have been the subject of extensive study since the foundational work of Döhler [1] because of their unique electronic and optical properties. By creating a periodic structure of alternating n- and p-doped layers of this semiconductor, the resulting electronic and optical properties of the superlattice are fundamentally altered from those of the bulk semiconductor [2]. The most striking features by which they differ from their compositional counterparts and from any homogeneous bulk semiconductor, is the strong tunability of their electronic structure and, consequently, of the resulting electrical

and optical properties [3]. This tunability arises from an *indirect gap in real space*, since the lowest conduction-band states are shifted by half a superlattice spacing with respect to the uppermost valence-band states. This shift is induced by the space-charge potential of the impurities. By varying the electron and hole concentration, the space-charge is also changed, and this in turn induces strong changes of the effective energy gap E_g^{NIPI}, which is always smaller than the gap of the homogeneous, bulk semiconductor material. Another interesting feature is the fact that electron-hole recombination lifetimes may exceed the corresponding values of bulk material by many orders of magnitude because of a small overlap of electron and hole states. This allows large deviations of electron and hole concentration from equilibrium values, even at extremely low excitation intensities. Any semiconductor, which can be n and p doped, can be used as a host material for the *n-i-p-i structure*. This is in contrast to the compositional superlattices, where the requirement of lattice matching severely restricts the choice of materials. Furthermore, any value of the effective bandgap $E_g^{eff,0}$ of the *n-i-p-i* crystal in the ground state (*i.e.* unexcited) that is smaller than the gap of the host material, E_g^0, can be generated by an appropriate choice of the design parameters, i.e., the doping concentration and the thickness of the layers.

3.2 Theoretical Considerations on Doping Superlattices

3.2.1 The Band Structure of Superlattices

In a crystalline solid, the periodicity is established by the regular arrangement of atoms in the crystal lattice, and hence, the period is dictated by the lattice constant of the particular solid [9]. In a superlattice crystal, the periodic sequence of layers which have alternating composition or doping, results in a new periodic variation of the electronic properties in the direction perpendicular to the layers (the superlattice direction). Whereas the lattice constant of a semiconductor is fixed, the superlattice period can be varied by changing the thickness of the layers.

The motion of the electrons parallel to the superlattice layers is, to a first

approximation, not affected by the periodic potential of the superlattice. The electrons moving in the superlattice direction are subject to a potential which has the superlattice period. The effect of this motion on the energy band structure of the host semiconductors is to limit the electron energy to narrow subbands due to the subdivision of the host *Brillouin* zone into a series of minizones. This is explained by refering to the dispersion relation in momentum space. The z-axis is chosen to lie along the superlattice direction. Figure 3.1 shows the dispersion curve $\epsilon(k_z)$ for the bulk semiconductor in the *Brillouin* zone defined by

$$|k_z| \leq \pi/a \tag{3.1}$$

where a is the lattice constant. The introduction of the superlattice periodicity has the effect of subdividing the *Brillouin* zone into a series of minizones, the first minizone defined by

$$|k_z| \leq \pi/d \tag{3.2}$$

where d is the superlattice period. It is obvious from the above relations that if the period d is much larger than the lattice constant a, then the minizone will be much smaller than the host *Brillouin* zone. The period of superlattice structures typically ranges from 20Å to 2000Å, which is equivalent to 4 to 400 lattice constants. In the reduced-zone scheme, the dispersion curve for the bulk semiconductor is folded back into the first *Brillouin* zone, using the translational symmetry properties of the crystal lattice. In an analogous manner, the dispersion curve $\epsilon(k_z)$ of the host semiconductors in the superlattice are folded back into the reduced *Brillouin* zone or minizone, and each host band is split into a number of minibands $\epsilon_n(k_z), n = 1, 2, 3, ...$, separated by forbidden gaps at the zone centre ($k_z = 0$) and the first minizone boundary ($k_z = \pm\pi/d$). Thus the most important consequence of the superlattice periodicity is the splitting of the conduction and valence bands of the host semiconductor into a series of minibands. These minibands are much narrower than the bands in a bulk seminconductor and the gaps between them are relatively large.

The band structure of a superlattice provides the environment for the observation of a number of high-field phenomena which are expected for the

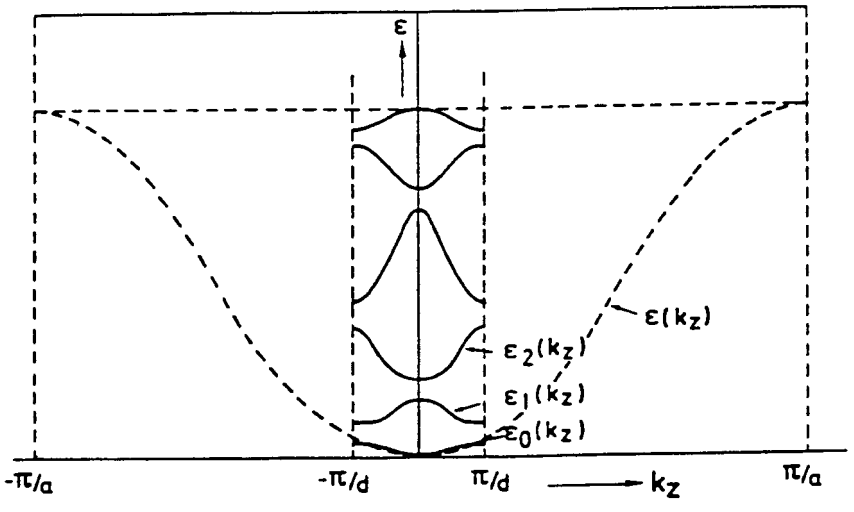

Figure 3.1: The dispersion curve of a bulk semiconductor as well as a superlattice.

periodic structures in general. These phenomena are usually not observable in any "natural" crystalline solid because the scattering of the free carriers by the electron-phonon and electron-electron interactions is too strong. The motion of the electrons is described by the so-called *Bloch* oscillations, which can in principle be observed in superlattices because of the excistence of minibands. In the presence of a strong electric field, the bands are tilted because of the potential difference which the field produces across the length of the crystal. The electrons are then accelerated by the electric field toward the upper edge of the tilted band (figure 3.2), and scattered after a time which is short compared to the time they require to attain the energy of the upper edge, and finally they lose the energy they have gained from the field by exciting thermal vibrations (phonons) in the crystal lattice. In the case of a superlattice, the excistence of minibands which are much narrower than the natural bands greatly increases the probability of an electron attaining the energy of the upper edge of a tilted miniband.

When the electrons attain this maximum energy, they are *Bragg* reflected and they acquire a negative velocity as they move towards the bottom edge

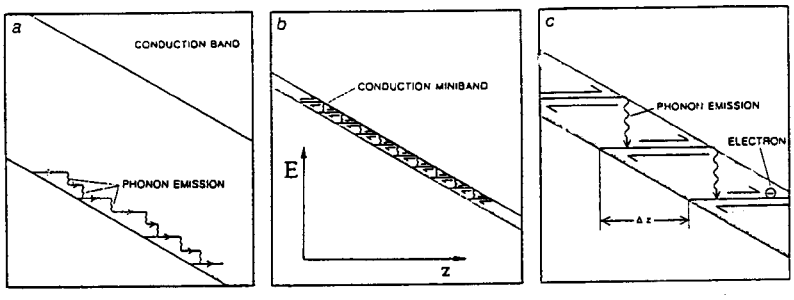

Figure 3.2: The motion of electrons in an applied electric field.
a) in the conduction band of a bulk semiconductor;
b) in the conduction miniband of a superlattice;
c) an enlarged section of b) showing the Bloch oscillations.

of the miniband. The electrons can be repeatedly *Bragg* reflected between the upper and the lower edges of the miniband, performing many *Bloch* oscillations before they are scattered, at which stage they relax to a lower energy in the miniband.

3.2.2 Electronic Structure

Doping semiconductor superlattices are composed of a periodic sequence of n- and p-type impurity layers, possibly with intrinsic regions between, in an otherwise homogeneous semiconductor [5]. They possess a space-charge-induced one-dimensional periodic potential which creates wells for electrons and holes, that are offset by one half-period (figure 3.3). This is in contrast to the compositional superlattices, where the different band gaps of the components induces periodic variations of the band edges. The fact that we are dealing with a homogeneous semiconductor which is only modulated by the superposition of a periodic superlattice potential, makes the theoretical treatment of the electronic structure easier. In general, the effective mass approximation provides a satisfactory description. The space-charge potential varies slowly over distances of the order of the bulk lattice constant and the considered energies of the bands are sufficiently close to the band edges. This

justifies the neglect of corrections due to the non-parabolicity of the bands.

A *n-i-p-i* crystal consists of an arbitrary homogeneous semiconductor with a periodic variation of *n*- and *p*-type doping,

$$n_D(z+d) = n_D(z); \quad n_A(z+d) = n_A(z) \tag{3.3}$$

where z is the direction of periodicity and d is the superlattice period [6]. An approximation was made, by replacing the space-charge distribution of the individual doping atoms with a homogeneous distribution function $e\,n_D(z)$ for donors, and $-e\,n_D(z)$ for acceptors. These distribution functions vary periodically in the superlattice direction. In making this approximation, the following have been neglected:

1. the spatial potential fluctuations which result from the random distribution of impurities in the doped regions, and
2. the point charge character of the impurities which may lead to bound impurity states or to the formation of impurity bands.

The motivation for this approximation is given by Ruden and Döhler [6]. The following is applicable in the case of GaAs doping superlattices,

1. the influence of potential fluctuations is reasonably small
2. donor impurity bands may be neglected, and
3. the formation of acceptor impurity bands must be considered within the typical range of values of design parameters of *n-i-p-i* crystals.

Long-range potential fluctuations are screened by a small concentration of free electrons in the n-type layers (holes in the p-type layers), making these fluctuations unimportant, if at least a certain fraction of the impurity space-charge per layer is compensated by free carriers. The short-range potential fluctuations result mainly from the random nearest-neighbour impurity distances, which deviate from the mean value r_m (the subscript m is valid for donors as well as acceptors). These fluctuations may be estimated by calculating the value of the unscreened *Coulomb* energy $e^2/\kappa_0 r_m$ of a point charge

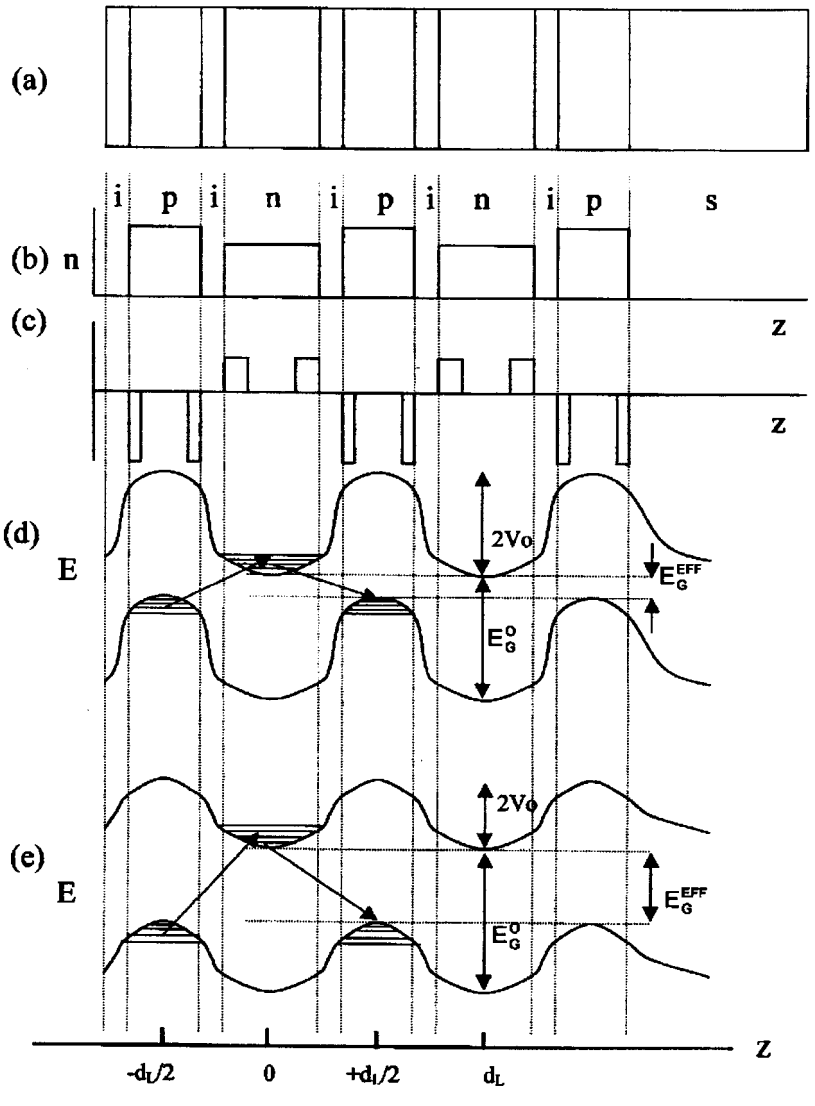

Figure 3.3: Physical and electrical structure of a doping superlattice.
a) p-doped, n-doped and intrinsic regions are indicated by p, n, and i respectively;
b) concentration of acceptors (n_A) and donors (n_D);
c) space-charge distribution;
d) modulation of conduction and valence bands by space charges - unexcited;
e) modulation of conduction and valence bands under optical excitation.

at a distance $r_m = [4\pi/(3n_m)]^{1/3}$, where κ_0 is the static dielectric constant of bulk GaAs. For any reasonable statistical distribution of the impurities, the width of the distribution will have roughly the value of the average. The numerical value of $e^2/\kappa_0 r_m$ increases from 15 to 32 meV within the range $5 \times 10^{17} cm^{-3} \leq n_m \leq 5 \times 10^{18} cm^{-3}$ with $\kappa_0 = 12.5$ for GaAs, which is always smaller than the corresponding subband energies. From this it is clear that, due to the screening by the charge carriers in the layers, the potential fluctuation will be reduced.

The importance of impurity bands may be estimated by the following argument. Consider a regular simple cubic array of n_m shallow impurities with ionization energy E_m, *Bohr* radius a_m, and nearest-neighbour distance $\tilde{r}_m = n_m^{-1/3}$. The impurity bandwidth would be approximately $12E_m exp(-\tilde{r}_m/a_m)$ in a tight-binding picture.

A different approach is based on the nearly-free-electron model. The kinetic energy at the *Brillouin* zone boundary becomes

$$\epsilon(\pi/\tilde{r}_m) \approx (\hbar^2/2m_e)\pi^2 n_m^{2/3} \tag{3.4}$$

A rough estimate of the band splitting is

$$2V(2\pi/\tilde{r}_m) \approx e^2/\kappa_0 \tilde{r}_m = e^2 n_m^{1/3}/\kappa_0 \tag{3.5}$$

The tight-binding picture is appropriate for $\tilde{r}_m \gg a_m$ whereas the nearly-free-electron model suits the case $\epsilon(\pi/\tilde{r}_m) \gg 2V(2\pi/\tilde{r}_m)$. Making use of an experimental value for the ionization energy of shallow donors in GaAs, $E_D \simeq 6meV$, which corresponds to a *Bohr* radius $a_D \simeq 10nm$, and using $m_e = 0.067m_0$ (m_e is the effective mass of an electron and m_0 is the rest mass of an electron), we get $\epsilon(\pi/\tilde{r}_D) \gg 2V(2\pi/\tilde{r}_D)$ for $n_D > 10^{16} cm^{-3}$. This shows that even the unscreened impurity potentials act as a relatively small perturbation at donor concentrations which are typical for *n-i-p-i* crystals. Therefore impurity-band formation in the case of the conduction band can be neglected, and it is allowed to replace the actual donor space charge by a homogeneous space charge distribution, $en_D(z)$.

In the case of the acceptor impurities we find (because of the larger heavy-hole effective mass m^{hh}) a *Bohr* radius $a_A \simeq 1.8nm$ so that $\tilde{r}_A > a_A$ for $n_A <$

$10^{20}cm^{-3}$ and $\epsilon(\pi/\tilde{r}_A) > 2V(2\pi/\tilde{r}_A)$ only if $n_A > 2 \times 10^{19}cm^{-3}$ using $m^{hh} = 0.6m_0$. This implies that an impurity band can exist in the p-type layers of a *n-i-p-i* structure, unless n_A is extremely high. This result does not signify that hole subbands do not exist in the p-type layers or that they are unimportant. The presence of an impurity band implies important consequences for the calculation of the self-consistent potential (to be discussed at a later stage).

The superlattice potential is exclusively space-charge induced. The reason for this is that the superlattice potential, in general, (also known as the space-charge potential) is made up of contributions by both the doping atoms (referred to as the bare ionized impurities or the fixed impurity charge) and the free-carriers (electrons and holes). (If the superlattice potential is calculated self-consistently, it is known as the self-consistent potential, $V_{SC}(z)$[2].) The superlattice potential is then defined as the sum of the fixed impurity charge potential and the free-carrier space charge potential[7]. The contribution of the fixed impurity charge to the superlattice potential $v_0(z)$ is determined by integrating *Poisson's* equation twice

$$\frac{\partial^2 v_0(z)}{\partial z^2} = \frac{4\pi e \rho_0(z)}{\kappa_0} \tag{3.6}$$

where $\rho_0(z) = e[n_D(z) - n_A(z)]$ and κ_0 is the static dielectric constant of the bulk semiconductor. *Poisson's* equation is also subject to the following boundary conditions [6]

$$\frac{\partial v_0(z)}{\partial z}\Big|_{z=0} = 0; \quad v_0(0) = 0 \tag{3.7}$$

This then gives

$$v_0(z) = \frac{4\pi e^2}{\kappa_0} \int_0^z dz' \int_0^{z'} dz''\{n_D(z'') - n_A(z'')\} \tag{3.8}$$

Except for the case of a compensated doping superlattice which contains the same amount of donors and acceptors per period d, *i.e.*,

$$\int_{-d/2}^{d/2} n_D(z)\, dz = \int_{-d/2}^{d/2} n_A(z)\, dz, \tag{3.9}$$

the condition of (macroscopic) neutrality of the crystal requires a periodic electron or hole space-charge distribution $-e\,n(z)$ or $e\,p(z)$ respectively. These

mobile charges provide a *Hartree*[1] [8] [9] contribution to the superlattice potential

$$v_H(z) = \frac{4\pi e^2}{\kappa_0} \int_0^z dz' \int_0^{z'} dz''\{-n(z'') + p(z'')\} \tag{3.10}$$

where $n(z)$ and $p(z)$ are the free electron and hole carrier densities respectively [2].

The exchange and correlation corrections of the free carriers also contribute to the superlattice potential. The exchange and correlation potential is obtained from[6]

$$v_{xc}(z) = \epsilon_{xc} n(z) + n(z)\frac{\delta \epsilon_{xc}}{\delta n} \tag{3.11}$$

where $\epsilon_{xc}(n)$ is the exchange and correlation energy per electron of a homogeneous electron gas of the (local) density n (this is the local density approximation of the density functional formalism [2]. Since the electronic densities of interest in *n-i-p-i* crystals are usually very high, *i.e.*, the mean distance between two electrons is short compared to the effective-mass *Bohr* radius $a_D^{EMA} = a_B \kappa_0 (m_0/m_{eff})$, we will take

$$-\epsilon_{xc} = -\epsilon_x = (0.916/r_s)(e^2/2\kappa_0 a_D^{EMA}) \tag{3.12}$$

with $r_s = [4\pi/(3n)]^{\frac{1}{3}}/a_D^{EMA}$. The inclusion of higher-order correlation terms does not affect the results appreciably. The contributions of the holes in the p-type layers to the superlattice potential is not written explicitly since it can be incorporated into the superlattice potential in the manner discussed above. [6]

Before proceeding further, it is necessary to make the following statements: [2] [5]

1. In a *compensated* doping superlattice, which contains the same amount of donors and acceptors per period d, the superlattice potential arises solely from the fixed impurity charges (or bare ionized impurities), and can be analytically determined with the help of *Poisson's* equation.

[1]The Hartree approximation replaces the dynamic interaction of an electron with the other electrons in a crystal, by averages of the interaction over the occupied electron states. This in effect, reduces the many-electron problem to a single electron problem, in which the *Schrödinger* equation containing the coordinates of only one electron, has to be solved.

2. In a *non-compensated* doping superlattice ($n_D d_n \neq n_A d_p$), the superlattice potential arises from both the fixed impurity layers and the excess free carriers (electrons and holes). This implies that the superlattice potential is the sum of the fixed-charge contribution (v_0), the *Hartree* contribution (v_H) of the free carriers, and the exchange and correlation corrections (v_{xc}) of the free carriers:

$$\begin{aligned} v_{SL}(z) &= \frac{4\pi e^2}{\kappa_0}\int_0^z dz' \int_0^{z'} z''\{n_D(z'') - n_A(z'')\} \\ &\quad + \frac{4\pi e^2}{\kappa_0}\int_0^z dz' \int_0^{z'} dz''\{-n(z'') + p(z'')\} \\ &\quad + 0.611\left(\frac{e^2}{\kappa_0}\right)\left(\frac{3n(z)}{4\pi}\right)^{\frac{1}{3}} \end{aligned} \tag{3.13}$$

Both the contributions of the free carriers have to be calculated self-consistently. This is in agreement with the *Hartree* approximation which reduces the many-electron problem to a one-electron problem.

Considering the non-compensated case, the self-consistent one-particle *Schrödinger* equation becomes

$$\frac{\hbar^2}{2m_{eff}}\frac{\partial^2 \Psi_{ikz}}{\partial z^2} + [E_i(k_z) - v_{sc}(z)]\Psi_{ikz} = 0 \tag{3.14}$$

where $v_{sc}(z)$ is the superlattice potential $v_{SL}(z)$, calculated self-consistently. To arrive at thè above equation, the following has to be kept in mind: it has been well established for semiconductor superlattices that charge carriers near the band edges behave as free carriers with an effective mass determined by the bulk band curvature, in the directions parallel to the superlattice layers, but are strongly perturbed in the direction of superlattice growth [5]. The envelope function approximation is used to separate the wave functions into bulk and superlattice components, and thus the subband energies and wave functions Ψ_{ikz} can be determined from the one-dimensional *Schrödinger* equation. Using the effective-mass approximation, the energy band structure of the superlattice is given by

$$E(k_z, k_t) = E_i(k_z) + \frac{\hbar^2 {k_t}^2}{2m_{eff}} \tag{3.15}$$

where E_i is the subband energy (i is the subband index) and k_z and k_t are the wave vectors perpendicular and parallel, respectively, to the superlattice layers (z being the direction of superlattice growth). In the next section the superlattice potential will be calculated for specific cases.

3.2.3 Superlattice Potentials

Compensated Superlattices

Consider the case of a *np* structure (therefore, no intrinsic layers between the n- and p-doped layers) with equal layer thickness d_n and d_p and constant doping concentration $n_D = n_A$. Thus in the ground state, the superlattice potential arises from only the ionized impurities and can be determined analytically from *Poisson's* equation [5]. First, consider a n-doped layer:

$$\frac{\partial^2 v_0(z)}{\partial z^2} = \frac{4\pi e \rho_n(z)}{\kappa_0} \tag{3.16}$$

where $\rho_n(z) = e n_D(z)$ and making use of

$$\int_{-d/2}^{d/2} n_D(z)\, dz = \int_{-d/2}^{d/2} n_A(z)\, dz. \tag{3.17}$$

Integrating twice, gives

$$\begin{aligned} v_{n0}(z) &= \frac{4\pi e^2}{\kappa_0} \int_0^{d_n/2} dz' \int_0^{z'} n_D(z'')dz'' \\ &= \frac{2\pi e^2}{\kappa_0} \left(\frac{d_n}{2}\right)^2 n_D \end{aligned} \tag{3.18}$$

Similarly, for a p-doped layer:

$$\begin{aligned} v_{p0}(z) &= \frac{-4\pi e^2}{\kappa_0} \int_{-d_p/2}^{0} dz' \int_0^{z'} n_A(z'')dz'' \\ &= \frac{2\pi e^2}{\kappa_0} \left(\frac{d_p}{2}\right)^2 n_A \end{aligned} \tag{3.19}$$

The amplitude of the compensated superlattice potential is then

$$V_{max} = \frac{2\pi e^2}{\kappa_0} \left[\left(\frac{d_n}{2}\right)^2 n_D + \left(\frac{d_p}{2}\right)^2 n_A \right] \tag{3.20}$$

Noncompensated Doping Superlattices

For noncompensated doping superlattices ($n_D d_n \neq n_A d_p$), the superlattice potential arises from both the ionized impurities and the excess free carriers. The one-dimensional superlattice potential is [2]

$$\begin{aligned} v_{SL}(z) &= \frac{4\pi e^2}{\kappa_0}\int_0^z dz' \int_0^{z'} [n_D(z'') - n_A(z'')]\, dz'' \\ &\quad + \frac{4\pi e^2}{\kappa_0}\int_0^z dz' \int_0^{z'} [-n(z'') + p(z'')]\, dz'' \\ &\quad - 0.611\frac{e^2}{\kappa_0}\left[\frac{3n(z)}{4\pi}\right]^{\frac{1}{3}} \end{aligned} \tag{3.21}$$

where the second and the third term are the *Hartree* and the *exchange and correlation* contributions respectively. The superlattice potential then has to be solved self-consistently, as it depends on the solutions of the one-particle *Schrödinger* equation. This is accomplished using iterative techniques.

3.3 Photoreflectance of Superlattices

The results of *Aspnes* (discussed in section 2.2.2) will now be applied to superlattices [12]. We begin by recalling that the confining potential (*i.e.* the superlattice potential) is along the z- or superlattice direction. Also, the wave function can be written as the product of an envelope function $F_n(z)$ and a *Bloch* state $u_{c0}exp(i\bar{k}\cdot\bar{r})$ representing the unconfined directions. Because of the confining potential, k_z is no longer an eigenvalue of the system, therefore (2.25) has to be modified:

$$\begin{aligned} \epsilon(E,\Gamma) &= 1 + \frac{8\pi^2 i e^2 \hbar}{m^2 E^2 L}\sum_{nm}\int_{BZ} dk^2 \int_0^\infty dt |\bar{e}\cdot\bar{p}_{cv}(\bar{k}) I_{nm}|^2 \\ &\quad \times \exp\left[\int_{-t/2}^{t/2} dt' \frac{i[E - E_{cv}^{nm}(\bar{k}) + i\Gamma]t'}{\hbar}\right] \end{aligned} \tag{3.22}$$

where n and m are the subband indices of the conduction and valence bands, L is the width of the confined region, and I_{nm} is the overlap integral between the electron and hole envelope functions (subband states). The sum over the subband states takes the place of the k_z integral in (2.25). If an electric field

is applied along the direction of confinement, the shape of the confining potential changes, and if the field is small, new quasibound states are formed. Furthermore, the new potential redistributes the electronic charge in such a manner that electrons and holes are localized at opposite ends of the confining region. Unlike the three-dimensional case, the new potential does not accelerate the particles and, hence, does not produce a continuously changing energy. The difference between the free and confined particles in an electric field can be viewed classically in the following manner. Under the influence of the additional force of the electric field, the electron is accelerated and its energy becomes time-dependent in that it will continuously change in time. This implies that at any two different times, the energy of the electron is not the same. In the confined case, the electric field acts to change the shape of the potential, thus at any two times, the energy of the particle is unchanged because it is in a quasibound state. The main effect of the field is to change the energy level, the functional forms of the wave functions, and the lifetime of the particle [10] [11]. Calculations have shown that for small fields, the energy changes by a fixed amount rather than in a continuous fashion as it would in the case of a free particle.

These results are very important because they indicate that one cannot replace $\bar{k}$ with $\bar{k} + e\bar{F}t/\hbar$ in (2.25). Instead, the interband energy $E_{cv}^{nm}(\bar{k})$ and the overlap integral between electrons and holes, I_{nm}, should be changed by some fixed amount that is not dependent on the time t. The energy changes to $E_{cv}^{nm}(\bar{k}) + \delta E_{cv}^{nm}$ and the overlap integral changes to $I_{nm} + \delta I_{nm}$. The quantities δE_{cv}^{nm} and δI_{nm} can be calculated from stationary-state perturbation theory.

Provided that δE_{cv}^{nm} is much smaller than any other energy present in the problem and that $\delta I_{nm}/I_{nm} \ll 1$, one can expand the exponent and the overlap integral to obtain

$$\begin{aligned} \epsilon &= 1 + \frac{iA'}{E^2} \sum_{nm} |I_{nm}|^2 \left(1 + \frac{2\delta I_{nm}}{I_{nm}}\right) \int_{BZ} dk^2 \int_0^\infty dt \left(1 + \frac{it\delta E_{cv}^{nm}}{\hbar}\right) \\ &\quad \times \exp\left\{\frac{i[E - E_{cv}^{nm}(\bar{k}) + i\Gamma]t}{\hbar}\right\} \end{aligned} \tag{3.23}$$

where $A' = 8\pi^2 e^2 \hbar |\bar{e} \cdot \bar{p}_{cv}|^2 / m^2 L$. Evaluating the integral over t and keeping

only first-order terms in the perturbation leads to

$$\begin{aligned}\epsilon(E,F,\Gamma) &= 1+\frac{iA'}{E^2}\sum_{nm}|I_{nm}|^2 \\ &\quad\times\int_{BZ}dk^2\left[\frac{i\delta E_{cv}^{nm}}{(E-E_{cv}^{nm}(\bar{k})+i\Gamma)^2}\right. \\ &\quad\left.+\frac{(1+2\delta I_{nm})/I_{nm}}{E+E_{cv}^{nm}(\bar{k})+i\Gamma)}\right] \end{aligned} \tag{3.24}$$

Equation (3.24) is the general result for any type of one-dimensional confining potential with the field applied along the confinement direction. The first term under the integral represents changes in ϵ from electric-field-induced changes in the gap, E_{cv}^{nm}, while the second term is a combination of the unperturbed dielectric function and a term due to the modulation of the overlap integral. Note that the modulated terms are first derivatives and not third derivatives as in the bulk case. Equation (3.24) can be expressed in a compact manner as a first derivative functional form for the modulated dielectric function

$$\Delta\epsilon=\left[\frac{d\epsilon}{dI_{nm}}\frac{dI_{nm}}{dF}+\frac{d\epsilon}{dE_{cv}^{nm}}\frac{dE_{cv}^{nm}}{dF}+\frac{d\epsilon}{d\Gamma}\frac{d\Gamma}{dF}\right]\Delta F \tag{3.25}$$

which is the most general form of the modulated dielectric function for confined systems.

References

[1] Döhler G.H., Phys. Stat Sol.(b) **52**, (1972a), p.79; Döhler G.H., Phys. Stat. Sol. (b) **52**, (1972b), p.533

[2] Ploog K., Döhler G.H., Advances in Physics **32**(3), (1983), p.285

[3] Döhler G.H., Künzel H., Ploog K., Phys. Rev. B**25**(4), (1982), p.2616

[4] Jensen P.N., (MSc) A Study of Semiconductor Superlattices : Characterization of Gallium Arsenide Doping Superlattices, (1989)

[5] Choquette K.D., Misemer D.K., McCaughan L., Phys. Rev. B**43**(9), (1991), p.7040

[6] Ruden P., Döhler G.H., Phys. Rev. B**27**(6), (1983), p.3538

[7] Schrüfer K., Eckl S., Metzner C., Beyer H.J., Döhler G.H., J. Appl. Phys. **72**(10), (1992), p.4992

[8] Davydov A.S., Quantum Mechanics, p.352

[9] Blakemore J.S., Solid State Physics (second edition), p.203

[10] Miller D.A.B. *et al.*, Phys. Rev. B**32**(2), (1985), p.1043

[11] Bastard G., Phys. Rev. B**25**, (1982), p.7584

[12] Glembocki O.J., Shanabrook B.V., Superlattices and Microstructures **5**(4), (1989), p.603

Chapter 4

Experimental Photoreflectance

4.1 General Technique

A schematic drawing of a typical experimental arrangement is shown in figure 4.1. Light from a broadband light source passes through a monochromator and is focused onto the sample (this will be referred to as the *probe-beam*). The sample is also illuminated by a laser beam that passes through a mechanical chopper operating at a frequency Ω_m. This chopped laser provides the modulation for photoreflectance (this will be referred to as the *pump-beam*). The *probe-beam* is reflected from the sample and focused onto a suitable detector. Notice that a filter is placed in front of the detector that blocks any diffusely reflected or scattered laser light. The light striking the detector contains two signals: the *dc* (or average value) which is proportional to the *dc* reflectance R of the material, and an *ac* signal which is proportional to the change in reflectance ΔR, produced by the modulation of the sample. The *ac* signal from the detector is measured by the lock-in amplifier (LIA) and recorded by a computer, while the *dc* signal is used as an input to the server motor which varies the *Variable Neutral Density Filter* (VNDF) to keep the *dc* signal constant, by varying the intensity of the *probe-beam*. This is a normalization technique which yields a derivative-like $\Delta R/R$ spectrum (the next section will be devoted to the normalization procedure) [1] [2] [3] [4].

A common problem associated with photoreflectance is the unwanted

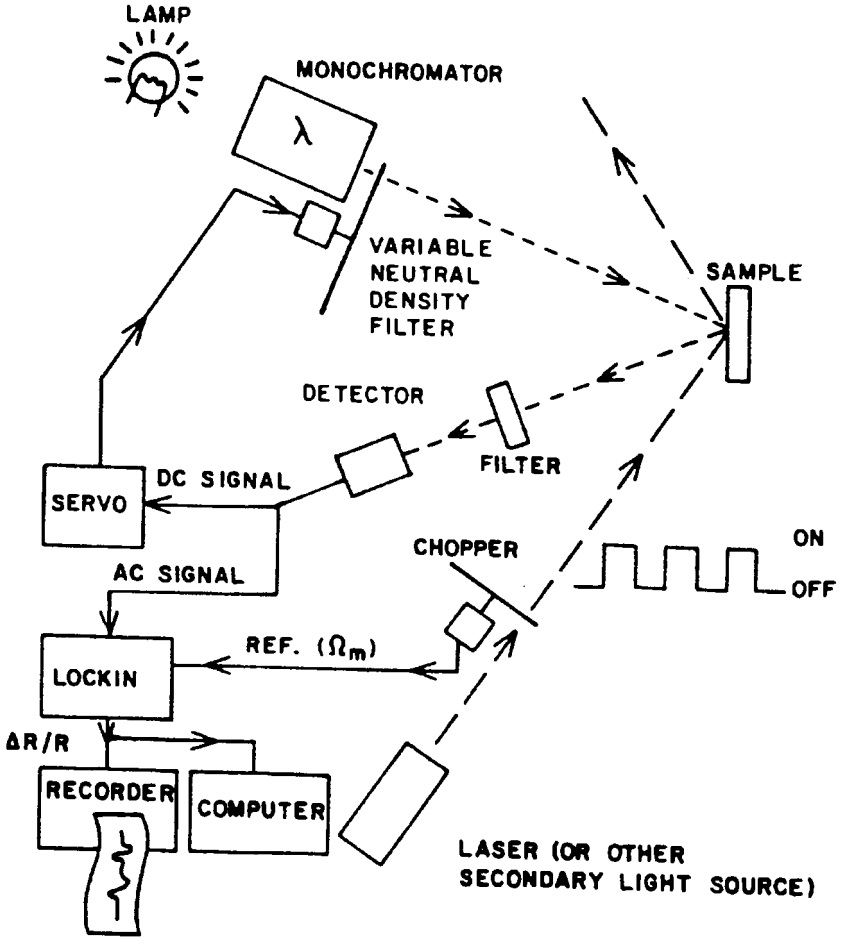

Figure 4.1: Schematic diagram of the photoreflectance apparatus.

(spurious) signal that enters the detector due to the diffusely reflected or scattered pump light, as well as possible photoluminescence. The photoluminescence signal is particularly accute at low temperatures, especially for superlattices and quantum wells (even at room temperature) [2]. Such signals are phase-locked to the modulation source and if not treated properly, can distort the PR spectrum, leading to erroneous results [5] [6]. The normalization procedure attempts to solve this problem.

4.2 Normalization Procedure

The technique will now be discussed in detail. The *dc* output of the detector V_{dc} can be written as

$$V_{dc} = I_0(\lambda)R(\lambda)K(\lambda)A(\lambda) \tag{4.1}$$

where $I_0(\lambda)$ is the light intensity striking the sample, $R(\lambda)$ is the *dc* reflectivity of the sample, $K(\lambda)$ is the detector response and $A(\lambda)$ is the amplification factor of the detector. The *ac* output is given by

$$V_{ac} = [I_0(\lambda)\Delta R(\lambda)K(\lambda) + I_{sp}(\lambda_{sp})K(\lambda_{sp})]A(\lambda) \tag{4.2}$$

where I_{sp} is the intensity of the spurious signal discussed in the previous section and λ_{sp} is the wavelength of the spurious signal. The second term in the above equation is generally absent in other forms of modulation spectroscopy. Since it is the quantity $\Delta R/R$ that is of interest in photoreflectance, it is necessary to eliminate the common factor $I_0(\lambda)$ (*i.e.*, keep $V_{dc}(\lambda)$ constant). The simplest method of elimination is to measure ΔR and R independently and to divide, but this presents problems due to the spurious-signal term [2]:

$$\frac{V_{ac}}{V_{dc}} = \frac{\Delta R(\lambda)}{R(\lambda)} + \frac{I_{sp}(\lambda)K_{sp}(\lambda)}{I_0(\lambda)R(\lambda)K(\lambda)} \tag{4.3}$$

This method will be suitable only if I_{sp} is very small.

In figure 4.1 normalization is achieved by means of the variable neutral density filter (VNDF), connected to a servo (or stepper) motor, placed in the optical path between the probe monochromator and the sample. The *dc* signal from the detector $[V_{dc}(\lambda)]$ is used as input to the servomotor, which varies

the VNDF and hence keeps V_{dc} as a constant. The method used in this study used the *dc* output of the detector to adjust the intensity of the broadband light source. The *dc* output was fed to a feedback-control unit which regulated the constant-voltage power supply that powered the light source.

4.3 Experimental Details

4.3.1 Experimental Setup

The broadband light source used is a commercial 50 watt Tungsten-halogen lamp. Power is supplied to this lamp by a constant-voltage power supply which is controlled by a feedback-control loop via the *dc* signal from the detector. The light is focused onto the monochromator-slit by a single lens. The light exiting the monochromator is then focused onto the sample (this is the *probe-beam*), and another lens collects the reflected light from the sample and focuses it onto the detector. A holographic notch-filter is placed in front of the detector to attenuate diffusely reflected or scattered laser light. The laser light source is a 633.8nm *He-Ne* laser that is focused onto the sample (this is the *pump-beam*). It should be noted that the *probe-beam* and the *pump-beam* are incident at different angles. Before the *pump-beam* reaches the sample, it passes through a chopper blade, which modulates the *pump-beam* at the modulation frequency, Ω_m. The chopper is phase-locked to the lock-in amplifier (LIA). The *dc* signal from the detector is fed to the differential input of the feedback-control loop, while the *ac* signal is recovered by the LIA. From there the output of the LIA is passed onto the personal computer (PC), which stores the data and is also responsible for controlling the monochromator.

The PC is equipped with a "PC30" A/D card, which establishes communication between the monochromator and LIA, and the PC. The control software is included in Appendix A. The file "PC30.CPP" is the driver software for the A/D card. The software has four main functions, namely initiating the A/D card, reading a single analogue value and converting it to a digital signal, and both a 12-bit and a 8-bit converter to convert digital signals to analogue output signals. The file "PC30G.CPP" is the user interface. It en-

ables the operator to select the scan interval of the monochromator and reads and stores the measurements received from the LIA. It also draws a real-time graph of the measurements against the wavelength of the monochromator.

4.3.2 General Precautions

Some precautions that have to be taken when doing measurements, will be discussed here:

1. The purpose of the *pump-beam* is to excite the carriers prevalent in the area of incidence. Therefore, the spot size of the *pump-beam* should be bigger or equal to the *probe-beam* spot size, and also, coincident, to have a modulation effect on the area of the sample being probed. The photon energy of the *pump-beam* should of course be above the energy gap of the semiconductor under investigation, to be able to lift carriers into the conduction band.

2. The modulation frequency Ω_m should never be a multiple of 50Hz as interfering signals will enter into the circuitry via the power-line input (the LIA will lock onto the experimental signal as well as the 50Hz *ac* signal). It is also advisable to switch on and adjust the chopper to the required frequency about an hour prior to the first measurements to be taken, in order to stabilize at the required frequency.

3. The mirrors used for directing the *pump-beam* to the sample should be mounted on stable mirror-mounts to ensure that the *pump-beam* is incident on exactly the same spot throughout the experiment.

4. Because the *He-Ne* laser has a 50kHz power supply, care should be taken in the positioning of the laser with respect to the steel, optical bench and/or the circuitry, as signals can be capacitively coupled (electrostatic coupling) onto wires in the circuit or electromagnetically coupled to wires acting as small antennas for electromagnetic radiation. Signal currents from one part of a circuit can couple to other parts through voltage drops on ground lines or power supply lines.

References

[1] Shen H., Dutta M., J. Appl. Phys. **78**(4), (1995), p.2151

[2] Shen H., Parayanthal P., Liu Y.F., Pollak Fred H., Rev. Sci. Instrum. **58**(8), (1987), p.1429

[3] Yan D., Qiang H., Pollak Fred H, Rev. Sci. Instrum. **65**(6), (1994), p. 1988

[4] Bhattacharya R.N., Shen H., Parayanthal P., Pollak Fred H., Phys. Rev. B**37**(8), (1988), p.4044

[5] Glembocki O.J., Shanabrook B.V., Proceedings of the Society of Photo-Optical Instrumentation Engineers (SPIE, Bellingham, 1987), Vol. 794, p.74

[6] Glembocki O.J., Proceedings of the Society of Photo-Optical Instrumentation Engineers (SPIE, Bellingham, 1990), Vol. 1286, p.2

[7] Shay J.L., Phys. Rev. B**2**(4), (1970), p.803

Chapter 5

Experimental Results

5.1 Photoreflectance Results of GaAs

5.1.1 Introduction

For the purpose of illustrating the technique of photoreflectance, two different GaAs samples were studied. They are:

1. sample 1 (figure 5.1): GaAs that was n-doped with Si at a level of $1 \times 10^{16} cm^{-3}$ (the sample consisted of a $6\mu m$ thick epitaxial GaAs layer on a bulk GaAs substrate) and,

2. sample 2 (figure 5.2): n-type GaAs (also Si-doped) with a net carrier concentration of $6.5 \times 10^{16} cm^{-3}$.

It is the aim of this section to demonstrate that the PR structure at the fundamental edge in GaAs results from a modulation of the electric field in the *Schottky* surface barrier by the photoexcited carriers. To accomplish this, the PR line shape, as a function of doping concentration, of the two samples, will be compared.

The experimental setup described previously was used to carry out all the measurements, with the chopper frequency set at 220Hz. The photoreflectance of each sample was measured at room temperature, for energies ranging between $1.2eV$ and $1.9eV$. Before discussing the results, it is necessary to briefly describe the depletion region *Schottky* barrier at the surface of

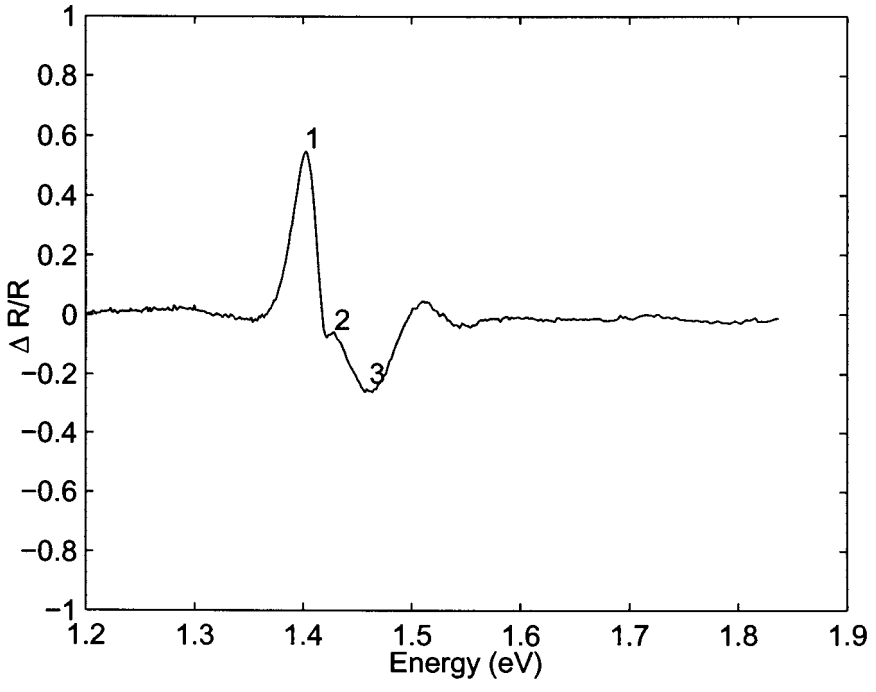

Figure 5.1: PR spectrum of Sample 1.

an extrinsic semiconductor, as it will help to predict the essential features of the experimental data.

Consider the potential distributions near the surface of an n-type GaAs sample. Figure 5.3 shows the electric field in the depletion region near the surface of an n-type semiconductor. The photoexcited electrons and holes find themselves in a strong electric field, that separates them, and this separation then reduces the built-in field. With the *pump-beam* off, the electric field varies linearly with distance from a maximum value E_{max} at the surface, to zero at a depth d below the surface. These quantities are given by

$$E_{max} = (2eN_d\varphi/\epsilon)^{\frac{1}{2}}, \tag{5.1}$$

$$d = (2\epsilon\varphi/eN_d)^{\frac{1}{2}}, \tag{5.2}$$

where N_d is the doping density, ϵ is the dielectric constant, and the potential difference φ, is the total amount of band bending. Since the spacing of

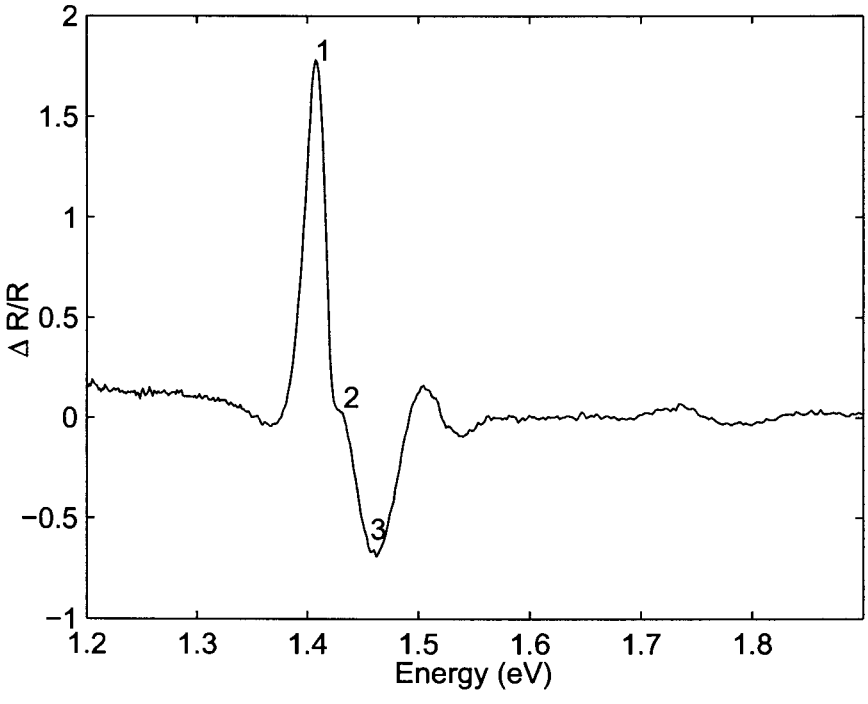

Figure 5.2: PR spectrum of Sample 2.

peaks in the *Franz-Keldysh* lineshape [1] is proportional to $E^{2/3}$ and (5.1) predicts that the maximum field increases as $N_d^{1/2}$, the spacing of peaks in the PR lineshape should vary as $N_d^{1/3}$. Shay [1] reported a discrepancy, where the experimentally obtained spacing between peaks were about half the predicted spacing. The same phenomenon was observed in sample 1 and sample 2. The predicted variation in the spacing of the peaks (1) and (2), is obtained by calculating the ratio between the respective carrier concentrations:

$$\left(\frac{N_{d,3}}{N_{d,2}}\right)^{\frac{1}{3}} = \left(\frac{6.5 \times 10^{16} cm^{-3}}{1 \times 10^{16} cm^{-3}}\right)^{\frac{1}{3}} \approx 1.87. \tag{5.3}$$

The experimentally observed spacing was determined as ≈ 0.95, which is about half of the predicted value. Shay [1] contributed this discrepancy to the fact that the impurity concentration in a sample might be considerably larger than the free-electron concentration. Therefore, the neutral donors or compensated acceptors below the Fermi level in the bulk can contribute to the effective doping density N_d, even though they do not contribute free carriers in the bulk.

5.1.2 Results and Discussion

The aim is to calculate the respective band gap energies from these experimental spectra, and compare the results to the band gap energy (E_g) of bulk GaAs, which is usually quoted as 1.424 eV at 300K [2]. To accomplish this, we refer to section 2.2.4, where, according to *Aspnes* [3][4], the band gap energy always lies between the two extrema, regardless of the value of the phase θ. The three-point method is used to calculate the position of the band gap between these two extrema. The extrema are indicated on the respective figures by the numbers 1 and 3. Using (2.56), (2.57), and (2.58), and also the plot of the scaling parameter $f(\rho)$ (figure 2.3), the band gap energies, E_{gi} of samples 1 and 2 are calculated as $E_{g1} = 1.447eV$ and $E_{g2} = 1.4525eV$ respectively. The large deviations of the E_{gi} values from the band gap value of bulk GaAs, could be attributed to the Franz-Keldysh theory, that predicts that an increase in the electric field, causes structure both below and above the band gap to

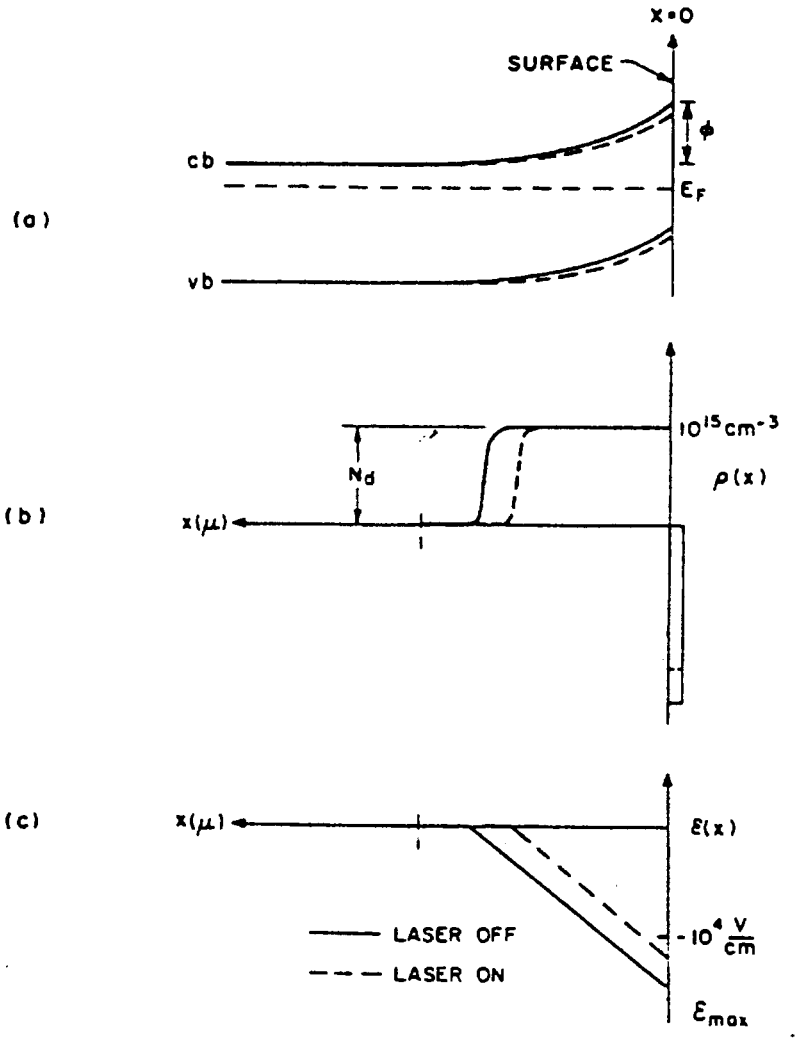

Figure 5.3: Schottky barrier depletion region at a semiconductor surface. C_b, V_b and E_F represent the conduction band, valence band, and Fermi energy respectively.

a) Bending of the energy bands,

b) the charge density as a function of depth x into the crystal, and

c) the macroscopic electric field as a function of depth into the crystal.

"move away" from the actual band gap [1]. Another possible cause of this deviation could be the uncertainty in the exact position of the $\Delta R/R = 0$ level of the PR response, as the relative peak values used to calculate the assymetry ratio ρ, are referenced to the $\Delta R/R = 0$ level. Furthermore, the scaling parameter $f(\rho)$ is determined graphically from figure 2.3, using the calculated value of ρ, which could introduce inaccuracy.

Another interesting feature present in both spectra is the kink (point 2) between the two main extrema. In the case of sample 1 the kink is at 1.425 eV and in the case of sample 2 the kink is at 1.428 eV. Estrera *et al* [5] reported a similar feature which they, together with Sydor *et al* [6] attributed to exiton/impurity effects. There is also an interesting relation between the indicated extrema for each of the samples. The extrema E_i display a periodicity with $(E_i - E_g)^{3/2}$. If this is plotted against the extremum number, a linear dependence is obtained. Both spectra show strong oscillatory behaviour above the GaAs band gap, which is characteristic of the FK effect observed in bulk material [7]. The linear dependence of the extrema confirms the identification of the spectral features as FK oscillations [8].

5.2 Photoreflectance Results of GaAs Doping Superlattices

5.2.1 Introduction

The samples studied in this section are three different doping superlattices, grown by organo-metallic vapour phase epitaxy (OMVPE) [9]. These superlattices are "n-p-n-p" structures with no intrinsic layers between the n- and p-doped layers (figure 5.4). The thicknesses of the n- and p-doped layers are denoted by d_n and d_p respectively.

The superlattice period for the "np" structures is

$$d = d_n + d_p. \tag{5.4}$$

The thicknesses for the n- and p-doped layers are the same $d_n = d_p = d$,

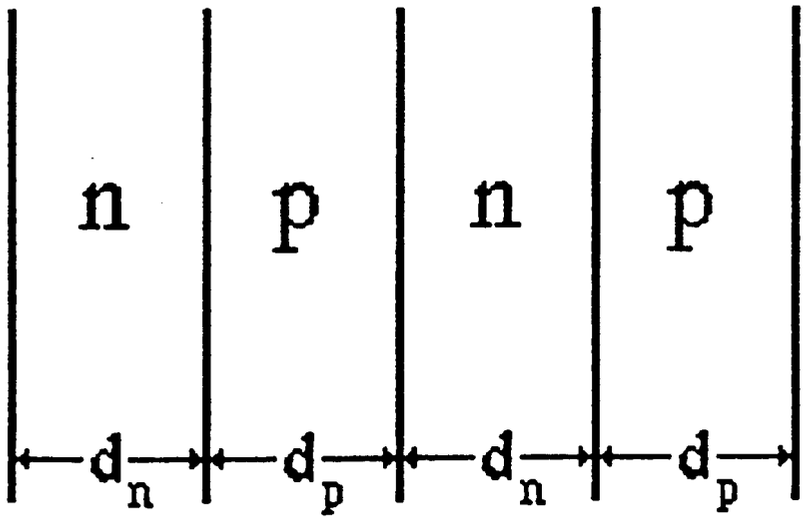

Figure 5.4: The layer sequences in the "np" doping superlattices.

with $d_1 = 600$ Å (superlattice 1), $d_2 = 400$ Å (superlattice 2), and $d_3 = 200$ Å (superlattice 3). The number of periods grown in each superlattice was chosen so that all the superlattices have the same total thickness of $2.40\mu m$. The smallest layer thickness was chosen to be 200 Å, because in thinner layers there are an insufficient number of carriers to produce a significant space charge potential for band modulation. Also, the layer thicknesses were chosen in multiples of 200 Å so that there will be an appreciable difference in the optical properties of the structures. The n-layers were doped with tellurium atoms to yield a donor concentration of

$$n_D = 1.0 \times 10^{18}\, atoms/cm^3 \tag{5.5}$$

and the p-layers were doped with zinc atoms to yield an acceptor concentration of

$$n_A = 1.0 \times 10^{18}\, atoms/cm^3. \tag{5.6}$$

The doping concentrations were chosen to be as high as possible in order to

Sample	$d_n = d_p$ (Å)	Amplitude (V)	Effective Band Gap (eV)
SL1	600	0.651	0.121
SL2	400	0.289	0.845
SL3	200	0.072	1.279

Table 5.1: The amplitude and effective bandgap of sample superlattices.

produce a large space-charge potential at the p-n interfaces, and thus achieve a large modulation of the host band structure. In all the samples an undoped GaAs buffer layer $0.5\mu m$ thick was first deposited on the substrate, followed by a p-doped layer and with the last layer being n-doped. Due to the transfer of electrons from the donor atoms in the n-layers to the acceptor atoms in the p-layers, the periodic layer sequence gives rise to a periodic space-charge potential in the doping superlattice. This space-charge potential induces a periodic modulation of the conduction and valence bands. The amplitude of the space-charge potential, with the assumption that there is complete transfer of the electrons from the n-doped layers to the p-doped layers, (V_0) is calculated using [9]:

$$V_0 = \frac{en_D d_n^2}{8\epsilon_0\kappa_0}, \tag{5.7}$$

where $d_n = d_p$ and $n_A = n_D$ (compensated superlattice), and the band gap of GaAs is taken as 1.424 eV. The amplitude as well as the effective bandgap, $E_g^{eff} \approx E_g - 2eV_0$ [10] were calculated and the results given in table 1.

The description of the superlattice samples is extended by a model for the charge distribution of the superlattice layers. The central regions, with thicknesses d_n^0 and d_p^0, are assumed not to be depleted of their carriers and are therefore conducting. The remaining parts of the layers of thicknesses $2d_n^+$ and $2d_p^-$ are the space-charge regions which border on the interfaces. The space-charge regions result from the transfer of electrons from the donor atoms in the n-layers to the acceptor atoms in the p-layers. This model is illustrated in figure 5.5 [9].

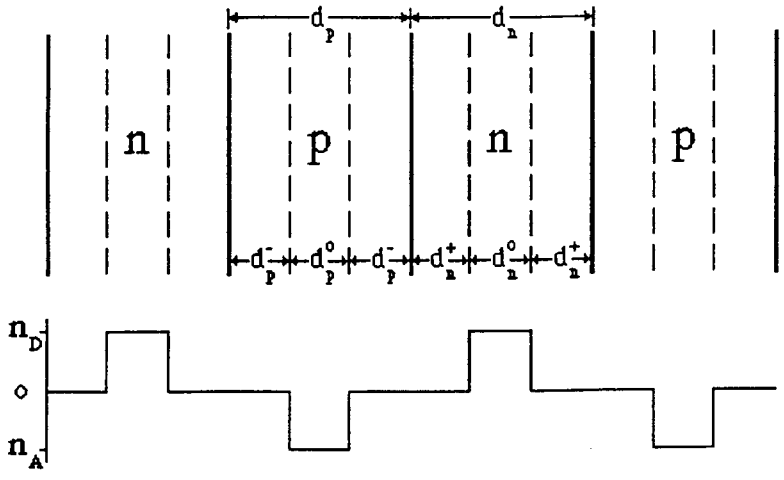

Figure 5.5: Schematic illustration of the model for the doping SL layers.

Sample	$d_n = d_p$ (Å)	d_n^0 (Å)
SL1	600	210
SL2	400	88
SL3	200	46

Table 5.2: Conducting layer thicknesses *vs.* the physical thicknesses.

Jensen [9] carried out resistivity and Hall effect measurements on both homogeneously-doped GaAs epilayers as well as the superlattices. Resistivity is determined measuring the sheet resistivity of the material and taking the product with the thickness of the sample. The Hall measurements also include making use of the thickness of the sample. Jensen observed deviations between the epilayers and superlattices which were corrected by using, instead of the physical thicknesses of the superlattice layers, the thickness d_n^0 of the conducting regions. The conducting layer thicknesses d_n^0 versus the physical thicknesses are given in table 2

The space-charge potential and the effective band gap can now be recalculated by replacing the physical layer thickness d_n with the total depletion

Sample	$d_n = d_p$ (Å)	$2d_n^+$ (Å)	Amplitude (V)	Effective Band Gap (eV)
SL1	600	390	0.275	0.874
SL2	400	312	0.176	1.072
SL3	200	154	0.043	1.338

Table 5.3: Recalculated amplitude and effective bandgap of sample superlattices.

layer thickness $2d_n^+ = d_n - d_n^0$ in (5.7). The results are given in table 3.

5.2.2 Results and Discussion

Photoreflectance measurements were carried out using the experimental arrangement described in sections (4.3) and (5.1.1). In the first phase of the study, the PR spectra of the superlattice samples described in section (5.2.1) were obtained. In the second phase, a superlattice sample similar to SL 3 were used to study the effects of α-particle irradiation, and subsequent annealing, on the PR spectra.

Non-Irradiated Samples

The PR spectra of the three samples are shown in figures (5.6), (5.7), and (5.8). All three spectra are characterized by well defined peaks both above and below the band gap of GaAs. These peaks represent transition energies. We know that in the case of bulk materials, the PR response has a third-derivative functional form (TDFF), where the main modulation mechanism is the field modulation of the surface potential. It is suggested that the modulation of the PR response of doping superlattices is not related to the surface potential, but rather to internal field modulation.

These materials have a two-dimensional subband structure in which the electrons and holes exist, *i.e.*, the potential wells for the electrons are located in the n-type layers, and the potential wells for the holes are located in the p-

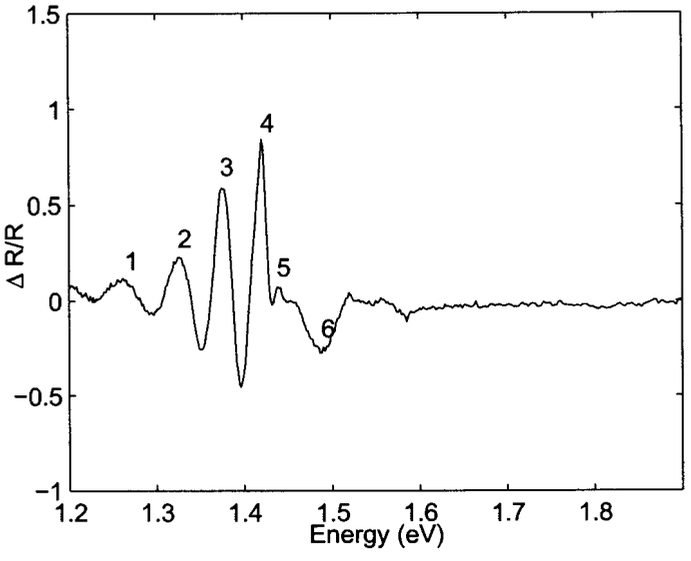

Figure 5.6: PR spectrum of SL 3.

type layers. When a pump beam is incident on the sample, the built-in potentials is modulated due to the modulation of the photo-excited carriers. However, because of the large carrier effective mass in the superlattice direction (growth direction), the characteristic electro-optic energy $\hbar\Omega$ produced by the built-in electric field in this direction, would be very small [11]. Therefore the TDFF mechanism has a small influence on the modulation of the dielectric function, and the modulation of the subband shift has a first-derivative functional form (FDFF).

Tang *et al* [11] have studied a sample very similar to SL 3, the only differences being the number of periods (15 as opposed to 60 for SL 3), and the growth process (MBE instead of OMVPE for SL 3). They calculated the built-in potential as 145 meV, which indicates that they assumed total depletion of the superlattice layers. There are two main differences between the results of Tang and the results for SL 3. In the case of Tang the cluster of peaks are mainly located above the band gap of bulk GaAs, and also, the peak spacing is very irregular. The spectrum of SL 3 shows three pronounced peaks just below the band gap of bulk GaAs, with the peak spacing being constant from

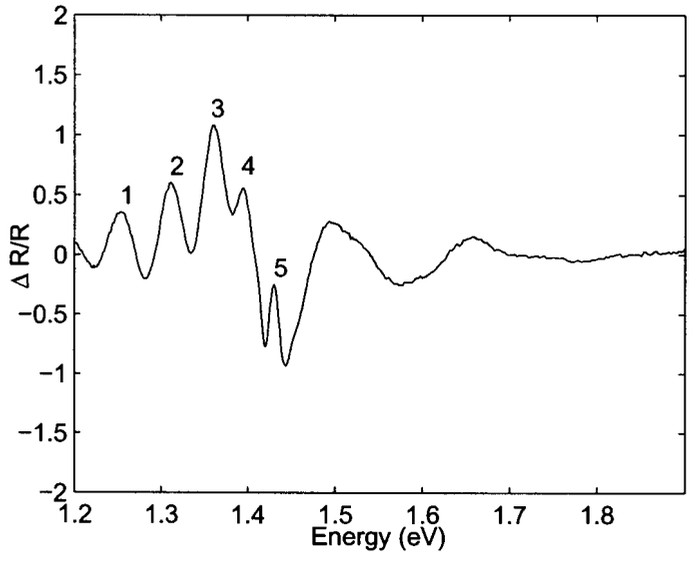

Figure 5.7: PR spectrum of SL 2.

peak (1) to peak (3). It is unclear whether peak (3) (at 1.42 eV) or peak (4) (at 1.44 eV), corresponds to the band gap of bulk GaAs.

Moving on to SL 2, we again see the most prominent peaks below the band gap of bulk GaAs. The peak spacing decreases gradually from (1) to (5). Peak (5) (1.43 eV) corresponds well with the band gap. Tang *et al* recorded PR spectra at different pump beam intensities and established that with decreasing pump beam intensity, additional structures were observed.

The PR spectrum (figure 5.9) of SL 2 was also recorded with a lower pump beam intensity, by inserting a 30% transmission filter in the path of the He-Ne laser beam. (The feature just above 1.4 eV is due to experimental error, where the A-D converter was not set correctly.) Comparing this spectrum with figure 5.7, we see that no additional structures appeared in the spectrum. In the case of Tang *et al* a 1 mW He-Ne laser was used, compared with the 5 mW He-Ne laser used in this study. It can be concluded, that, even with a 30% transmission filter, the intensity of the pump beam was still too high to observe the reported effect.

Next, we consider SL 1. This sample shows a PR response that is very

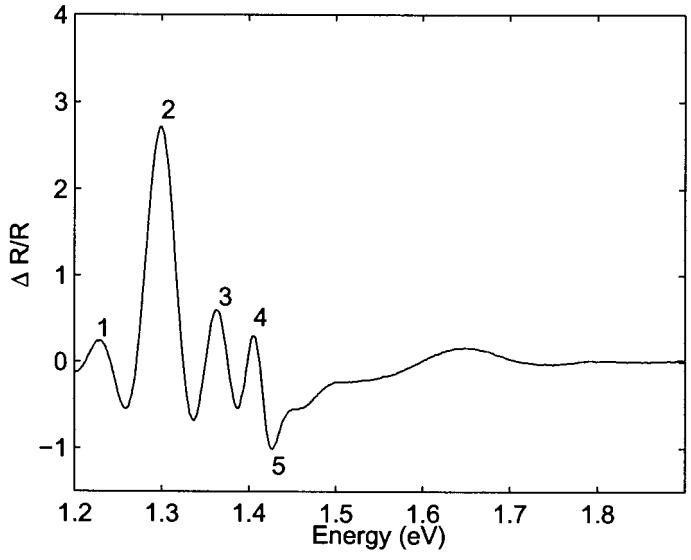

Figure 5.8: PR spectrum of SL 1.

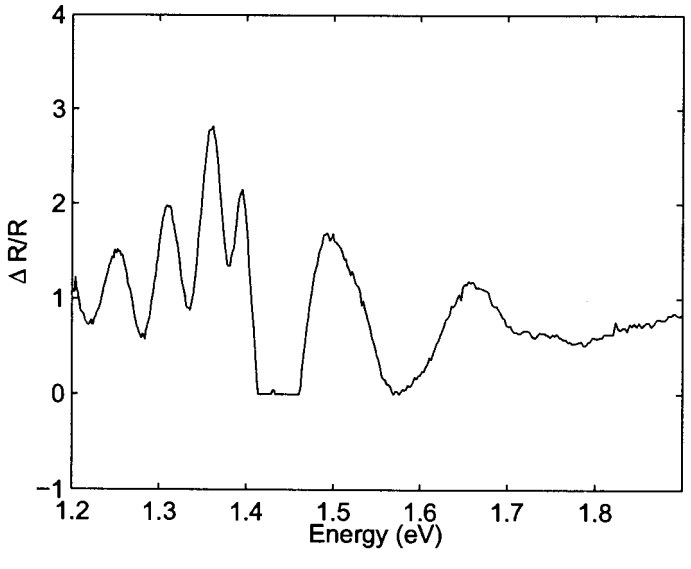

Figure 5.9: PR spectrum of SL 2 with 30% transmission filter.

similar to SL 2. Again, the most prominent peaks are situated below the bulk band gap, with the peak spacing decreasing from peak (1) to (5). The only indication of the bulk band gap is the negative peak (5) at $1,425$ eV.

Before proceeding further, it is important to make a few general remarks regarding the interpretation of the spectra.

1. The measured PR response is a function of how the probe as well as the pump beam is focussed onto the sample under study. With the equipment available, there was no way of ensuring that the different samples were measured under identical conditions.

2. Before each measurement, a pre-scan was done to determine where the strongest peak is, and then the lock-in amplifier was "locked" onto this signal.

From the above remarks, one can come to the conclusion that it is difficult to compare the relative intensities of the peaks in a PR spectrum, and to compare peaks from different spectra with each other.

Returning to the issue of the functional form of the PR lineshape. Shen *et al* [12] reported room temperature measurements on two different samples, where the samples had built-in potentials of 1.2 eV and 85 meV respectively. They ascribed the PR features of the sample with the large built-in potential to Franz-Keldysh oscillations. The sample with the small built-in potential had a number of features both below and above the band gap of GaAs, and they ascribed these to the transitions between the quantized electron and hole states. Comparing their work with the results obtained in this study, we see that SL 3 has a built-in potential of 86 meV, and therefore, according to their conclusions, is a case of internal field modulation.

Irradiated Samples

For the purpose of studying the effects of irradiation and subsequent annealing, a superlattice similar to SL 3 has been irradiated with an α-particle source. The sample has been irradiated for 90 minutes in total, and after that annealed for a total of 4 hours at different temperatures (1 hour at a time).

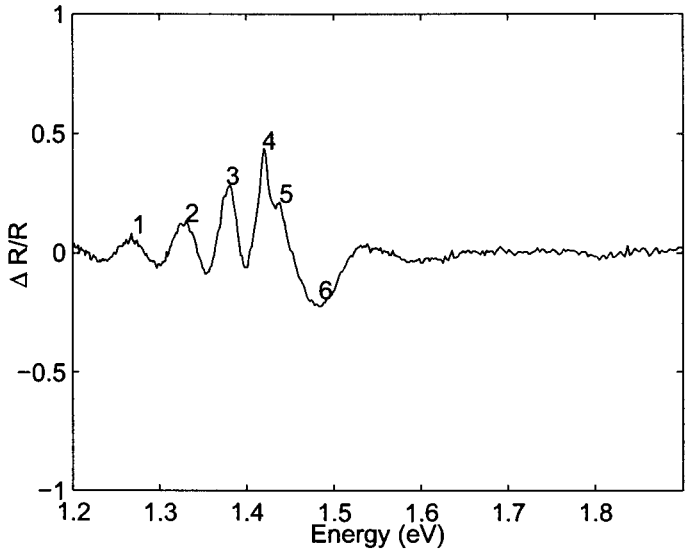

Figure 5.10: PR spectrum after 15 min. irradiation.

A control measurement was done on the sample before the irradiation treatment commenced, to determine whether the PR response corresponds to that of SL 3 or not. After each irradiation treatment, the PR spectrum was measured, with the results shown in figures 5.10, 5.11, 5.12, and 5.13. The sample was then annealed four times, one hour at a time. The annealing temperature ranged from 460 to 640 K.

Comparing the peaks on the PR spectrum, before irradiation and after the irradiation treatment, it is evident that the irradiation did not have any effect on the number of distinguishable peaks, or on the position of these peaks. The annealing process did have a noticable effect on the PR spectra. The spectrum obtained after the first annealing process (figure 5.14), shows extreme tilting of the PR response, together with, what seems to be noise. However, after annealing at a temperature of 640 K, the PR response returns to normal, indicating complete recovery of the superlattice.

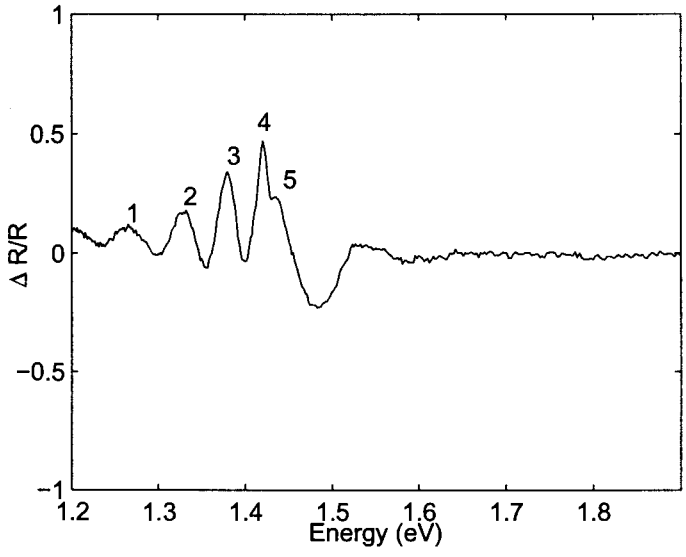

Figure 5.11: PR spectrum after 30 min. irradiation.

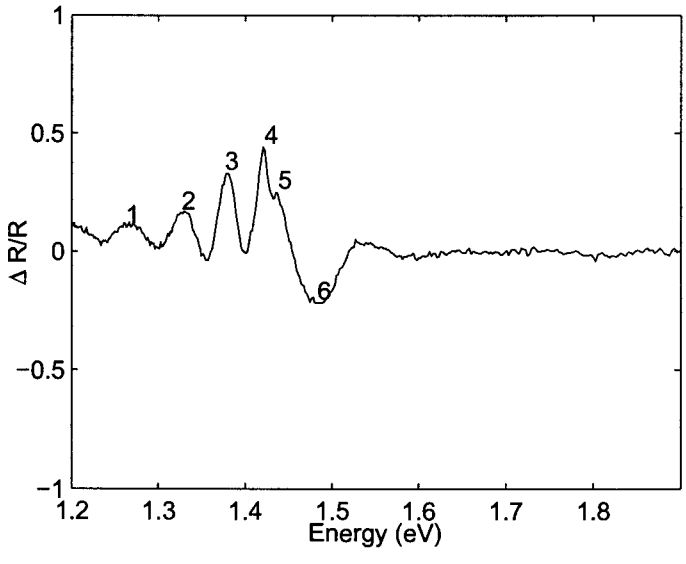

Figure 5.12: PR spectrum after 60 min. irradiation.

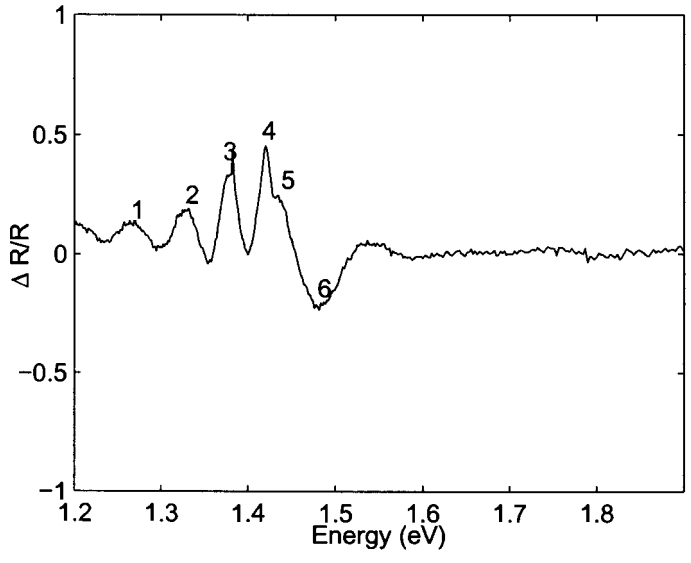

Figure 5.13: PR spectrum after 90 min. irradiation.

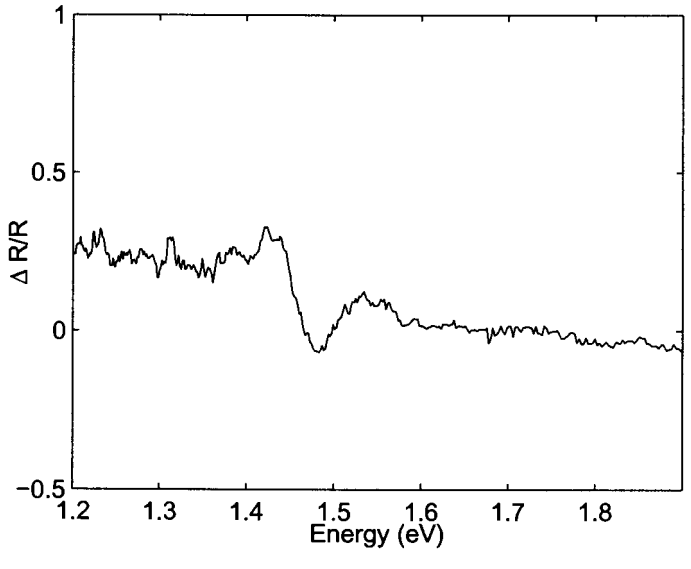

Figure 5.14: PR spectrum after 1 hour of annealing (460K).

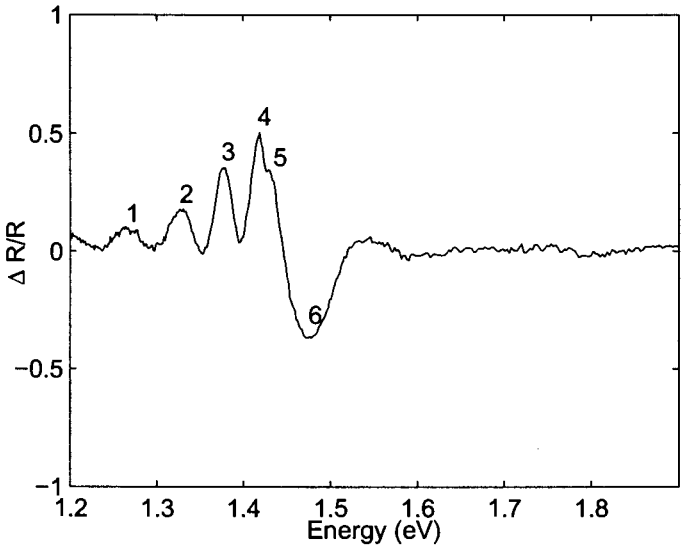

Figure 5.15: PR spectrum after 4 hours of annealing (640K).

References

[1] Shay J.L., Phys. Rev. B**2**(4), (1970), p.803

[2] Sydor M., Engholm J.R., et al, Phys. Rev. B**49**(11), (1994), p.7306

[3] Aspnes D.E., Surf. Sci. **37**, (1973), p.418

[4] Aspnes D.E., Rowe J.E., Phys. Rev. Lett. **27**(4), (1971), p.188

[5] Estrera J.P., Duncan W.M., Glosser R., Phys. Rev. B**49**(11), (1994), p.7281

[6] Sydor M., Angelo J., Wilson J.J., Mitchel W.C., Chen M.Y., Phys. Rev. B**40**, (1989), p.8473

[7] Aspnes D.E., Studna A.A., Phys. Rev. B**10**, (1973), p.4605

[8] Enderlein R., Scolfaro L.M.R., Martins J.M.V., Leite J.R., Superlattices and Microstructures **12**(2), (1992), p.175

[9] Jensen P.N., "A Study of Semiconductor Superlattices: Characterization of Gallium Arsenide Doping Superlattices", (1989)

[10] Ploog K., Döhler G.H., Advances in Physics **32**, (1983), p.285

[11] Tang Y., Wang B., Jiang D., Zhuang W., Liang J., Solid State Comm. **63**(9), (1987), p.793

[12] Shen X.C., Shen H., Parayanthal P., Pollak F.H., Superlattices and Microstructures **2**(6), (1986), p.513

Chapter 6

Conclusion

This study indicates that it is relatively easy to implement the technique of photoreflectance and that the amount of information obtainable, can be considerable. However, the measured lineshapes are complicated and require careful analysis which have to be aided by the theoretical treatment of PR. Of all the modulation techniques, PR yields the sharpest structure, and this fact makes it useful when investigating new materials or microstructures which are characterized by complex electronic transitions.

In essence, PR represents the optical response of a system to the applied modulation. This implies that important information lies in the other modulation variables such as the phase, the modulation frequency, the modulation amplitude and the pump wavelength used. The technique used for this study can be expanded and improved in the following way:

1. As mentioned in section (5.2.2), it is important to carry out all measurements under exactly the same conditions. This implies accurate placement of samples, accurate focusing and positioning of the probe as well as the pump beam, and measurement and control of the pump beam intensity.

2. If the above mentioned conditions are met, it will be possible to measure PR responses under different modulating conditions and compare results.

3. Measuring under different modulation conditions can sometimes decrease the signal level to such an extent that the signal becomes partially buried under the noise floor. Therefore, a signal processing approach wil have to be followed in order adjust experimental parameters (such as the time constant and sensitivity of the lock-in amplifier) correctly and in general, to describe measured data in a statistically correct way.

4. Two modulating conditions that could be varied fairly easily, are the chopping (modulation) frequency and the intensity of the pump beam. The idea is then to study the effect on the amplitude of the PR peaks as well as the number and position of peaks in the spectrum. A particularly interesting problem would be to determine the oscillator strengths of different transitions.

5. The interpretation of the effect irradiation and annealing has on the PR response calls for a study aimed specifically at this effect. To aid in the interpretation it might be necessary to obtain information on the changes in the material parameters, as this will aid in the understanding of the changes in the PR response.

Appendix A

C codes

A.1 Software driver for the A/D card

Pc30.cpp

```
/* PROGRAM OM A/D KAART TE BEDRYF
v1.2   Mei/Junie 1991
v1.5   Oktober 1996
*/

#include<stdio.h>    /* standaard C funksies */
#include<dos.h>      /* poort adresering */
#include<ctype.h>    /* to-upper() */
#include<conio.h>    /* getch() */

void pc_mmenu();
void pc_init();
void pc_clrAD();
void pc_wrt12(double val);
void pc_wrt8(double val);
double pc_rdAD();
void pc_puls12(double val);
```

```
void pc_wait(int peri);

struct sbyte        /* struktuur gee veranderlikes van lengte = 1 bit */
  {
  unsigned int b0:1;     /* 1 bit lengtes */
  unsigned int b1:1;
  unsigned int b2:1;
  unsigned int b3:1;
  unsigned int b4:1;
  unsigned int b5:1;
  unsigned int b6:1;
  unsigned int b7:1;
  };

union bnum          /* 8 opeenvolgende 1-bit veranderlikes word by        */
  {                   /* dieselfde adres as 'n 1 byte veranderlike gestoor */
  struct sbyte bb; /* 8 enkel bits */
  unsigned char wb;/* 1 byte */
  } bval;

double vin=0.0,v8=0.0,v12=0.0,p12=0.0;
unsigned int L8=2,L12=0,CHAN=0,LINE=12,error=0;
unsigned int ADDATL=0,ADDSR=1,ADCCR=2,ADMDE=3,TMRCTR=7,
  DIOCTR=11;
unsigned int OFFSET=0x700,DAC0=12,DAC1=16,DAC2=20,DAC3=21;
int rpt;


void pc_mmenu()                                          pc_mmenu
  {
    char tst;
    clrscr();
```

```
puts("********************* MAIN MENU ***************
 *****");
puts(""); puts("");
puts("DRUK 'n SLEUTEL SOOS AANGEDUI:");
puts(""); puts("");
printf("O: Kaartadres    = %X (%d)\n\n",OFFSET,OFFSET);
printf("I: Inlees spanning = %E  K: Kanaal =
  %d\n\n",vin,CHAN);
printf("U: Uitlees (8_bit) = %E  L: Lyn(2,3) =
  %d\n\n",v8,L8);
printf("V: Uitlees (12_bit = %E  C: Lyn(0,1) =
  %d\n\n",v12,L12);
printf("P: Puls (12 op C) = %E   G: Go puls\n\n",p12);
printf("F:    Fout status = %d          R:
  Reset fout\n",error);
puts("Q: QUIT");
tst=toupper(getch());
switch(tst)
  {
    case 'F': clrscr();
              if(error==1)
              {
                 puts("'n inlees fout is geraporteer");
                 puts(" herstel kaart deur -R- te roep");
              }
              else puts(" geen fout is geraporteer nie");
              puts(" druk enige sleutel om voort te gaan");
              getch();
              break;
    case 'R': pc_clrAD();
              break;
    case 'O': clrscr();
```

```
            printf("Offset adres (HEX) = ");
            scanf("%X",&OFFSET);
            break;
case 'K': clrscr();
            printf("Kanaal nr vir inlees = ");
            scanf("%d",&CHAN);
            break;                                          90
case 'V': clrscr();
            printf("Uitlees spanning met 12 bit op
             %ld (V) = ",L12);          scanf("%lG",&v12);
            pc_wrt12(v12);
            break;
case 'U': clrscr();
            printf("Uitlees spanning met 8 bit op
             %ld (V) = ",L8);
            scanf("%lG",&v8);
            pc_wrt8(v8);                                    100
            break;
case 'L': clrscr();
            printf("Lyn nr vir 8 bit uitlees (2,3) = ");
            scanf("%d",&L8);
            break;
case 'C': clrscr();
            printf("Lyn nr vir 12 bit uitlees (0,1) = ");
            scanf("%d",&L12);
            if(L12==0) LINE=12;
                else    LINE=16;                            110
            break;
case 'I': vin=pc_rdAD();
            break;
case 'P': clrscr();
            printf("pulsspanning = ");
```

```
                scanf("%lG",&p12);
                break;
        case 'G': pc_puls12(p12);
                break;
        case 'Q': rpt=0;                                        120
                clrscr();
                break;
        default : break;
      }
    }
      void pc_init()    /* Inisiering van AD kaart */          pc_init
{
  unsigned char lb;
  int ww;
    bval.bb.b7=1; bval.bb.b6=0; bval.bb.b5=0; bval.bb.b4=1;     130
    bval.bb.b3=0; bval.bb.b2=0; bval.bb.b1=1; bval.bb.b0=0;
    outportb(ADMDE +OFFSET,bval.wb);
    bval.bb.b7=0; bval.bb.b6=0; bval.bb.b5=1; bval.bb.b4=1;
    bval.bb.b3=0; bval.bb.b2=1; bval.bb.b1=0; bval.bb.b0=0;
    outportb(TMRCTR+OFFSET,bval.wb);
    bval.bb.b7=0; bval.bb.b6=1; bval.bb.b5=1; bval.bb.b4=1;
    bval.bb.b3=0; bval.bb.b2=1; bval.bb.b1=0; bval.bb.b0=0;
    outportb(TMRCTR+OFFSET,bval.wb);
    bval.bb.b7=1; bval.bb.b6=0; bval.bb.b5=1; bval.bb.b4=1;
    bval.bb.b3=0; bval.bb.b2=1; bval.bb.b1=1; bval.bb.b0=0;     140
    outportb(TMRCTR+OFFSET,bval.wb);
    bval.bb.b7=0; bval.bb.b6=0; bval.bb.b5=0; bval.bb.b4=0;
    bval.bb.b3=0; bval.bb.b2=0; bval.bb.b1=1; bval.bb.b0=0;
    outportb(ADCCR +OFFSET,bval.wb);
    bval.bb.b7=1; bval.bb.b6=0; bval.bb.b5=0; bval.bb.b4=1;
    bval.bb.b3=1; bval.bb.b2=0; bval.bb.b1=1; bval.bb.b0=1;
    outportb(DIOCTR+OFFSET,bval.wb);
```

```
    do
    {
      lb=inportb(ADDATL+OFFSET); /* lees van lb reset bit 6 van hb na 0 */
      bval.wb=inportb( ADDSR+OFFSET); /* lees ADDSR register */
     } while(bval.bb.b5==1); /* loop solank AD besig (bit 5) op is */
    ww=inport(ADDATL+OFFSET);/* lees nou 2 bytes=woord van AD */
    L8=2;pc_wrt8(0.0); L8=3;pc_wrt8(0.0);L8=2;   /* uitgange na nul */
    L12=0;LINE=12;pc_wrt12(0.0); L12=1;LINE=16;
    pc_wrt12(0.0);L12=0;LINE=12;
/*     puts("Alle uitgange is op 0 volt");
    puts("A/D-kaart is geinisieer");
    puts("druk 'n sleutel om voort te gaan");
    getch();*/
 }
       void pc_clrAD() /* roetine om AD skoon te maak */          pc_clrAD
 {
   unsigned char lb;
int ww;
      bval.bb.b7=1; bval.bb.b6=0; bval.bb.b5=0; bval.bb.b4=1;
      bval.bb.b3=0; bval.bb.b2=0; bval.bb.b1=1; bval.bb.b0=0;
      outportb(ADMDE +OFFSET,bval.wb);
      bval.bb.b7=0; bval.bb.b6=0; bval.bb.b5=0; bval.bb.b4=0;
      bval.bb.b3=0; bval.bb.b2=0; bval.bb.b1=1; bval.bb.b0=0;
      outportb(ADCCR +OFFSET,bval.wb);
    do
    {
      lb=inportb(ADDATL+OFFSET);
      bval.wb=inportb( ADDSR+OFFSET);
 } while(bval.bb.b5==1);
    ww=inport(ADDATL+OFFSET);
    error=bval.bb.b7;
 }
```

```
        double pc_rdAD()   /* roetine om enkel lees van AD te doen */ 180 pc_rdAD
{
  unsigned char lb,bb;
  int ww,dcode;
  bb=2+(CHAN<<4);              /* bb = ch3 ch2 ch1 ch0 0 0 1 0 */
  outportb(ADCCR+OFFSET,bb); /* skryf na ADCCR register */
  bb++;                        /* bb = dieselfde met strobebit=1 */
  outportb(ADCCR+OFFSET,bb); /* stap 1 van sagteware strobe */
  bb--;                        /* bb = soos voorheen met strobebit=0 */
  outportb(ADCCR+OFFSET,bb); /* stap 2 van sagteware strobe */
   do                                                          190
   {
     bval.wb=inportb( ADDSR+OFFSET);
   } while(bval.bb.b6==0);     /* loop tot bit 6 = 1 = klaar */
   lb=inport(ADDATL+OFFSET); /* bit 6 = klaar word gevee */
   ww=inport(ADDATL+OFFSET); /* lees woord van AD */
   error=bval.bb.b7;             /* bit 7 gee fout */
   dcode=ww-4096;
/*     dcode=ww-2048;*/
   return((dcode*10.0)/4096.0); /* bereken spanning: 0 - 10 V skaal */
/*  return((dcode*10.0)/2048.0); */ /* bereken spanning: -10 - +10 V skaal */ 200
}

void pc_wrt12(double val) /* 12-bit DA omsetter vir uitreeseine */    pc_wrt12
{
  unsigned int bcode;
  unsigned char lb,hb;
  bcode=2048-(val*204.8); /* bereken b-kode vir spanning: -10 - +10 V */
  hb=bcode>>4;             /* high byte van 12 bit kode */
  lb=(bcode<<12)>>8;     /* low byte: net 4 bits na links verskuif */
  outportb(OFFSET+LINE+1,hb); /* laai adres */                    210
  outportb(OFFSET+LINE,lb);  /* uitree met skryf van low byte */
```

```
  bval.wb=inportb( ADDSR+OFFSET); /* lees ADDSR vir moontlike fout */
  error=bval.bb.b7;                    /* noteer fout */
}
void pc_wrt8(double val) /* 8-bit DA omsetter vir uittreeseine */      pc_wrt8
{
  unsigned char bcode;
  bcode=128-(val*12.8);        /* bereken b-kode vir spanning: -10 - +10 V*/
  outportb(OFFSET+DAC2-2+L8,bcode); /* adres van uittreepoort */
  bval.wb=inportb( ADDSR+OFFSET); /* lees ADDSR vir moontlike fout */ 220
  error=bval.bb.b7;                    /* noteer fout */
}
        void pc_puls12(double val) /* huidige 12-bit uitgang kry puls tot   pc_puls12
          'val' en weer */
{                          /* terug na nul */
  pc_wait(10000);              /* wag 0.1 sek na sleutel gedruk is:
    minder geraas */
  pc_wrt12(val);              /* skryf spanning na uitgang */
  pc_wait(100);                /* verskaf puls se lengte = 1 ms */
  pc_wrt12(0.0);              /* uitgang terug na nul */                  230
}
        void pc_wait(int peri)                                          pc_wait
{
  int i,a=1,b=1;
  for(i=1;i<peri;i++)      a=a+(10*a+2*b)*10-(10*a+2*b)*10;
    /* bewerking om tyd te wen */
}
```

A.2 User interface for data acquisition

```
#include <stdio.h>
#include <string.h>
#include <conio.h>
```

```
#include <stdlib.h>
#include <ctype.h>
#include <graphics.h>
#include <dos.h>
#include <math.h>
#include "pc30.h"

#define MIN -1
#define ZERO 0
#define POS 1
#define PPULSE 2
#define NPULSE -2
#define WAIT  3
#define FSET 32 // Filter value
#define SIZE 2000

double F_UPPER=3.5,F_LOWER=3.0;
int FI_UPPER,FI_LOWER;

/*
   CH=0   : DA0 input    (grey)
   LINE=12 : CH0 output  (red)
   LINE=16 : CH1 output  (orange)
*/

void counter();
void stop();
void go_pos();
void go_neg();
```

```
unsigned int fpc_rdAD();
double diosig[SIZE]; // array to store signals from photodiode
long QANGSTROM=0,RWAIT=0,FSCALE=100;
double wstart,CWL,EOS,WLI;
double wave[SIZE];          // array to store wavelengths                    40
char EXIT=0, RSTATUS=0,RCOUNT=0, SCAN=0, SCAN_2=0;
double buf[1024],buf2[1024], flt=0, ftotal=0;
int ctr,index1,index2;      // indicates element number in array
int maxx,maxy;
double xmin,xmax,ymin,ymax;
double xdata,xinterval,ydata,yinterval,Energy;
int xcoord,ycoord;
FILE *leer;
char FILENAME[20];
                                                                            50


/*************************************************************************/
/* "plotgraph()" teken eksperimenteel gemete waardes vanaf fotodiode      */
/* teenoor golflengte van monochromator                                   */
/*************************************************************************/
void plotgraph()                                                  plotgraph
{
 xdata=wave[index2];
 Energy=12398.56/(xdata);                                                 60
 xinterval=ceil((Energy-1.20)*(58.00/0.20));
 xcoord=(100+xinterval);

 ydata=15*(diosig[index1]);
 yinterval=ceil((ydata)*(48.00/20.00));
 ycoord=(378-yinterval);
```

```
 lineto(xcoord,ycoord);
 index1++;
 index2++;                                                    70
}


/*************************************************************************/
/* "axes()" teken grafiek-asse en skryf onderskrifte/byskrifte by        */
/* onderskeie asse ?                                                     */
/*************************************************************************/
void axes()                                                   axes
{
 double Xint,xval;                                            80
// long int Yint;
 int XPixelDiff/*,YPixelDiff*/,i,j,yval;
 char stry[10];
 char *strx;
 int dec,sign,ndig=3;

 xmin=1.20; xmax=3.00; ymin=0.00; ymax=120.00;
 maxx=getmaxx(); maxy=getmaxy();
 Xint=(xmax-xmin)/9; //Yint=floor((ymax-ymin)/6);
 XPixelDiff=58; //YPixelDiff=maxy/10;                         90

 moveto(100,122); lineto(100,maxy-100);
 lineto(maxx-20,maxy-100);
 moveto(maxx-20,maxy-103);
 lineto(maxx-20,maxy-97);
 lineto(maxx-16,maxy-100);
 lineto(maxx-20,maxy-103);
 moveto(97,122);
 lineto(103,122);
```

```
  lineto(100,118);                                                    100
  lineto(97,122);

  for (j=0;j<=9;j++)
    {
     moveto(100+j*XPixelDiff,maxy-100); lineto(100+j*XPixelDiff,maxy-103);
     xval=xmin+j*Xint;
     strx=ecvt(xval,ndig,&dec,&sign);
     outtextxy(88+j*XPixelDiff,maxy-90,strx);
     outtextxy(200,maxy-70,"Photon Energy (eV)");
    }                                                                 110

   Energy=12398.56/(wstart);
   xinterval=ceil((Energy-1.20)*(58.00/0.20));
   xcoord=(100+xinterval);
   moveto(xcoord,378-yinterval);
}


/*************************************************************************/
/* Inisieer 'GRAPHICS.H'                                                 */ 120
/*************************************************************************/
void graph_init()                                                graph_init
{
 int gd,gm,err;

 detectgraph(&gd,&gm);
 initgraph(&gd,&gm,"c:\\bc\\bgi");
 if ((err=graphresult() ) !=grOk)
    {
     printf("Graphics init error: %s",grapherrormsg(err));          130
     exit(1);
```

```
    }
}

void count_header()                                          count_header
{
 clrscr();
 printf("Select operation:\n\n"
        " +      : Increase wavelength\n"
        " -      : Decrease wavelength\n"                    140
        " <SPACE> : Stop\n"
        " .      : Positive Pulse\n"
        " ,      : Negative Pulse\n"
        " C      : Calibrate\n"
        " S      : Scan\n"
        " <ESC>  : Quit\n\n");
}

void count_disp()                                            count_disp
{                                                            150
 char s[20];

 switch (RSTATUS)
   {
    case ZERO  : sprintf(s,"%c          ",254); break;
    case POS   : sprintf(s,"%c          ",16); break;
    case MIN   : sprintf(s,"%c          ",17); break;
    case PPULSE : sprintf(s,">>         "); break;
    case NPULSE : sprintf(s,"<<         "); break;
    case WAIT  : sprintf(s,"WAITING"); break;                160
   }

 gotoxy(1,12);
```

```
 printf("Status: %s\n",s);
 CWL=wstart+2*(float(QANGSTROM)/4.0);
 printf("Current wavelength: %.2lf  ",CWL);
}


void go_pos()                                          170 go_pos
{
 LINE=12; pc_wrt12(0.00);
 if (RSTATUS==MIN) delay(3000);
 LINE=16; pc_wrt12(5.00); RCOUNT=POS;
}

void go_neg()                                          go_neg
{
 LINE=16; pc_wrt12(0.00);
 if (RSTATUS==POS) delay(3000);                        180
 LINE=12; pc_wrt12(5.00); RCOUNT=MIN;
}

void stop()                                            stop
{
 if ((RSTATUS==POS) || (RSTATUS==MIN))
   {
    RSTATUS=WAIT;
    RWAIT=80000;
   }                                                   190
 else if ( (RSTATUS==PPULSE) || (RSTATUS==NPULSE) )
   {
    RSTATUS=WAIT;
    RWAIT=500;
   }
```

```
 else
 RSTATUS=ZERO;

 LINE=12; pc_wrt12(0.00);
 LINE=16; pc_wrt12(0.00);                                    200
}


void getscanval()                                            getscanval
{
 clrscr();
 printf("Current wavelength: %.2lf \n",CWL);
 printf("Scan to: ");
 scanf("%lf",&EOS);
 printf("Wavelength-interval(in Angstrom): ");               210
 scanf("%lf",&WLI);
 printf("Enter filename: ");
 scanf("%s",FILENAME);

 if (EOS>CWL)
   {
    RSTATUS=POS;
    go_pos();
   }
 else                                                        220
   {
    RSTATUS=MIN;
    go_neg();
   }
 count_header();
}
```

```
void count_scan()                                                    count_scan
{
 printf("\nScanning...\n");                                          230
 CHAN=1;
 printf("\nV_IN: %lf",pc_rdAD());
 diosig[index1] = pc_rdAD(); // reads signal from photodiode and stores
                             // in array
 fprintf(leer,"%E %E\n",wave[index2],diosig[index1]);
/* if (index2==1)
   {
    Energy=12398.56/wstart;
    xinterval=ceil((Energy-0.80)*(75.00/0.20));
    xcoord=(100+xinterval);                                          240
    ydata=5*(diosig[index1]);
    yinterval=ceil((ydata)*(48.00/20.00));
    ycoord=(380-yinterval);
    moveto(xcoord,ycoord);
   }*/
 plotgraph();

 CHAN=0;
 if (RSTATUS==POS)
   {                                                                 250
    if (CWL>=EOS) { SCAN=0; stop(); count_header(); count_disp(); }
   }
 else if (RSTATUS==MIN)
   {
    if (CWL<=EOS) { SCAN=0; stop(); count_header(); count_disp(); }
   }
 else { SCAN=0; count_header(); count_disp(); }
}
```

```
                                                                    260
void count_kbevent()                                                count_kbevent
{
 char c;

 if (RSTATUS==WAIT)
   {
    if (RWAIT) RWAIT--;
      else { RSTATUS=ZERO; count_disp(); }
    return;                                                         270
   }


 if (!kbhit()) return;

 c=toupper(getch());

 switch(c)
      {
       case 'C' : if (SCAN) break;                                  280
                  clrscr();
                  printf("Recalibrate wavelength (in ): ");
                  scanf("%lf",&wstart);
                  QANGSTROM=0;
                  count_header();
                  break;
       case 'S' : if (SCAN) break;
                  getscanval();
                  leer=fopen(FILENAME,"w");
                  SCAN=1;                                           290
                  graph_init();
```

```
                axes(); break;
        case '-' : if (SCAN) break;
                go_neg(); RSTATUS=MIN; break;
        case 32  : stop(); break;
        case '+' : if (SCAN) break;
                go_pos(); RSTATUS=POS; break;
        case '.' : if (SCAN) break;
                if (RSTATUS==ZERO)
                 {                                              300
                  RSTATUS=PPULSE;
                  count_disp();
                  go_pos(); delay(20);
                  stop();
                 } break;
        case ',' : if (SCAN) break;
                if (RSTATUS==ZERO)
                 {
                  RSTATUS=NPULSE;
                  count_disp();                                 310
                  go_neg(); delay(20);
                  stop();
                 } break;
        case 27 : stop(); EXIT=1; break;
       }

 count_disp();

}
                                                               320
// change v-in value to a 0->500 scale (100/Volt)
unsigned int fpc_rdAD()                                        fpc_rdAD
{
```

```
 buf2[flt]=pc_rdAD()*FSCALE;          //*500/5.0        // Update filter
 ftotal+=buf2[flt];
 if (flt<FSET) flt++; else flt=0;
 ftotal-=buf2[flt];

 return ftotal/FSET;
}                                                                    330



void counter()                                                       counter
{
   int x,y;
   unsigned int m;

   while ((fpc_rdAD()<FI_UPPER) && !EXIT) { count_kbevent(); }
   while ((fpc_rdAD()>FI_LOWER) && !EXIT) { count_kbevent(); }       340
   if (!EXIT)
     {
      QANGSTROM+=RCOUNT;
//       gotoxy(21,13);
      CWL=wstart+2*(float(QANGSTROM)/4.0);
      ctr++;
      if (ctr>=((WLI/2)*4))
        {
         ctr=0;
         gotoxy(21,13);                                              350
         printf("%.21f  ",CWL);
         wave[index2]=CWL;
         if (SCAN)
           {
            count_scan();
```

```
            }
        }
    }
}
                                                                    360
void count()                                                        count
{
 unsigned int i;

 for (i=0; i<640; i++) buf[i]=0;

 clrscr();
 printf("Enter current wavelength (in ): ");
 scanf("%lf",&wstart);
 QANGSTROM=0;                                                       370

 count_header();
 count_disp();

// leer=fopen(FILENAME,"w");
 do counter();
    while (!EXIT);
 fclose(leer);
 closegraph();
 clrscr();                                                          380
 printf("\nPC30 Control Program v1.0\n\n"
        "Type PC30 /? for help.\n");
}

void usage()                                                        usage
{
 printf("\nPC30 Control Program v1.0\n\n"
```

```
        "USAGE:\n"
        "     PC30 [-g] [-?]\n\n"
        "     -g   : Graphic mode, display input wave
                     for calibration\n"
        "     -s   : Enter calibration values\n"
        "     -?   : This help message\n\n"
        "Keys in graphic mode:\n"
        "     +    : Increase sample delay\n"
        "     -    : Decrease sample delay\n"
        "     t    : Toggle trigger mode on/off\n"
        "   <ESC> : Quit\n");
}

/*void setval(char *fname)
{
 FILE *fil;

 printf("\nPC30 Control Program v1.0\n\n"
        "Enter upper detection level (prev. %lf Volt): ",F_UPPER);
 scanf("%lf",&F_UPPER);
 printf("Enter lower detection level (prev. %lf Volt): ",F_LOWER);
 scanf("%lf",&F_LOWER);
 if ((fil=fopen(fname,"rb+"))==NULL)
   {
    printf("Error accessing .EXE file (Read-Only?)\n");
    exit(1);
   }
 fseek(fil,-16,SEEK_END);
 fwrite(&F_UPPER,1,8,fil);
 fwrite(&F_LOWER,1,8,fil);
 fclose(fil);
```

```
}     */                                                          420

/*void getval(char *fname)
{
 FILE *fil;

 if ((fil=fopen(fname,"rb"))==NULL)
    {
     printf("Error accessing .EXE file\n");
     exit(1);
  }                                                               430
 fseek(fil,-16,SEEK_END);
 fread(&F_UPPER,1,8,fil);
 fread(&F_LOWER,1,8,fil);
 fclose(fil);
}          */

void main()                                                       main
{
 pc_init();
 ctr=0;                                                          440
 index1=0;
 index2=0;
// getval(argv[0]);
 FI_UPPER=F_UPPER*100;
 FI_LOWER=F_LOWER*100;
/* if ( (argv[1][0]=='/') || (argv[1][0]=='-') )
    {
     switch (toupper(argv[1][1]))
       {
        case 'G' : graph(); break;                                450
        case 'S' : setval(argv[0]); break;
```

```
            case '?' : usage(); break;
            default  : usage(); break;
          }
        }
    else
        {*/
         count();

    return;                                                    460
}
```